Influence of circular RNA topology on microRNA stability

Federico Fuchs Wightman[1, 2*], Jerónimo Lukin[3*], Sebastián Giusti[3], Michael Soutschek[4, 5], Laureano Bragado[1, 2], Berta Pozzi[6], Paula González[7], Juan P. Fededa[7], Gerhard Schratt[4, 5], Damián Refojo[3#] & Manuel de la Mata[2, 8#]

[1]Universidad de Buenos Aires, Facultad de Ciencias Exactas y Naturales.

[2]CONICET-Universidad de Buenos Aires, Instituto de Fisiología, Biología Molecular y Neurociencias (IFIBYNE), Buenos Aires, Argentina.

[3]Instituto de Investigación en Biomedicina de Buenos Aires (IBioBA) - CONICET - Partner Institute of the Max Planck Society, Godoy Cruz 2390, C1425FQD Buenos Aires, Argentina.

[4]Lab of Systems Neuroscience, D-HEST Institute for Neuroscience, ETH Zürich, Switzerland.

[5]Neuroscience Center Zurich, ETH Zurich and University of Zurich, Switzerland.

[6]Institute of Cell Biology, University of Bern, Bern, Switzerland.

[7]Instituto de Investigaciones Biotecnológicas "Dr. Rodolfo A. Ugalde", IIB-UNSAM, IIBIO-CONICET, Universidad Nacional de San Martín, Buenos Aires, Argentina.

[8]Universidad de Buenos Aires, Facultad de Ciencias Exactas y Naturales. Departamento de Fisiología, Biología Molecular y Celular.

[*]Contributed equally.

[#]Correspondence: drefojo@ibioba-mpsp-conicet.gov.ar, mmata@fbmc.fcen.uba.ar.

Abstract

Circular RNAs (circRNAs) have been proposed to “sponge” or block microRNAs, a property shared with linear RNAs. Alternatively, certain RNAs induce microRNA destruction through the process of Target RNA-Directed MicroRNA Degradation (TDMD). Whether both linear and circular transcripts are equivalent in driving TDMD is unknown. Here we show that RNA topology seems critical for TDMD. Through a novel system that expresses a circRNA while reducing the co-expressed cognate linear RNA, we propose that circRNAs cannot induce TDMD. Interestingly, this appears attributed to the circular

RNA topology and not to its sequence, which is TDMD-competent in its linear form. Similarly, based on the previous knowledge that *Cdr1as* circular RNA protects miR-7 from Cyrano-mediated TDMD, we demonstrate that depletion of *Cdr1as* reduces miR-7 abundance, while overexpression of an artificial linear version of *Cdr1as* drives TDMD. By analysing RNA sequencing data of a neuron differentiation system, we detect potential events of circRNA-mediated microRNA stabilization. Our results support a model in which circRNAs, unlike linear mRNAs, lead to a topology-dependent TDMD evasion, aiding in the stabilization of specific microRNAs.

Keywords: circRNA/microRNA/TDMD

Introduction

Circular RNAs (circRNAs) are long known regulatory RNAs that have gained remarkable attention since the first reports that highlighted their high diversity and abundance (Memczak *et al*, 2013; Hansen *et al*, 2013; Salzman *et al*, 2013; Jeck *et al*, 2013). CircRNAs are covalently closed structures that originate from pre-mRNA backsplicing and therefore lack a poly-A tail and 5'-cap. As a result, given that these terminal modifications are the entry points for the microRNA (miRNA) effector machinery (Bartel, 2018; Jonas & Izaurralde, 2015), circRNAs seem largely immune to posttranscriptional degradation by miRNAs. Conversely, although current knowledge points towards a diversity of both nuclear and cytoplasmic functions for different individual circRNAs, several findings have suggested that some circRNAs regulate gene expression by working as miRNA "sponges" (Chen, 2020; Xiao *et al*, 2020; Hanan *et al*, 2020).

Whether circRNAs act on miRNAs by blocking them functionally, affecting their stability, or a combination of both remains to be determined. In particular, it is unclear whether circRNAs are active in driving Target Directed MicroRNA Degradation (TDMD), a mechanism that has emerged as central in affecting miRNA turnover. During TDMD, targets with extensive base-pair complementarity towards the 3' end of the miRNA –i.e. displaying no more than 3 mismatches in addition to a central bulge– lead to miRNA degradation, reversing the logic of canonical miRNA target silencing by which the target RNA is conventionally degraded (Ameres *et al*, 2010; Cazalla *et al*, 2010; Marcinowski *et al*, 2012; Fuchs Wightman *et al*, 2018). TDMD induces a conformational change on Argonaute (AGO) proteins that leads to their poly-ubiquitination and degradation, rendering the specifically loaded miRNAs unprotected

58 and susceptible to degradation by general nucleases (Shi *et al*, 2020; Han *et al*, 2020). Unlike sponging,
59 TDMD-inducing targets act catalytically even at sub-stoichiometric levels, resulting in the most selective
60 and potent miRNA degradation mechanism described to date and which seems to explain the half-lives
61 of most naturally unstable miRNAs (de la Mata *et al*, 2015; Denzler *et al*, 2016; Kleaveland *et al*, 2018; Shi
62 *et al*, 2020). A priori, the circular topology of circRNAs should not represent an impediment to regulating
63 miRNAs through TDMD, and circRNAs' high stability could even be an advantage for this activity.
64 Nevertheless, to date no circRNA has been described to drive TDMD and the only available evidence
65 indicates that circRNAs might instead lead to miRNA stabilization (Piwecka *et al*, 2017; Chen *et al*, 2019).
66 CircRNAs are typically coexpressed with their cognate linear RNAs from the common host genes.
67 However, the circRNA over linear ratio occurs in different proportions, with a subset of circRNAs
68 reaching higher levels than their cognate linear isoforms (Chen, 2020). To reveal insights into circRNA-
69 specific functions and mechanisms, a plethora of publications have relied on circRNA overexpression
70 using various inverted repeat-containing vectors (Zhang *et al*, 2014; Conn *et al*, 2015; Liang & Wilusz,
71 2014; Kramer *et al*, 2015; Li *et al*, 2017, 90; Liu *et al*, 2019; Guarnerio *et al*, 2019; Litke & Jaffrey, 2019;
72 Memczak *et al*, 2013; Hansen *et al*, 2013). Yet, the capability of plasmid-based methods to overexpress
73 exogenous circRNAs free from overlapping, "leaky" linear RNA expression remains questionable. Thus,
74 attributing any observed effects to the overexpressed circRNA while not rigorously controlling for the
75 potential role of the undesired coexpressed linear transcripts represents a potential pitfall (Pamudurti
76 *et al*, 2017; Kristensen *et al*, 2019; Dodbele *et al*, 2021; Chen, 2020).
77 A key general question in the field that remains largely unanswered, is whether the circular nature
78 of circRNAs is intrinsically or mechanistically linked to their molecular functions. In this study we aimed
79 to elucidate whether linear and circular target topologies function differently to affect miRNA stability
80 and function. Using a strategy that allows us to express an artificial circRNA with reduced expression of
81 the counterpart linear transcript, we showed that the circular RNA, as opposed to the linear form, seems
82 unable to induce TDMD. We also examined the well described *Cdr1as*-miR-7-Cyrano network of
83 noncoding RNAs, where the lncRNA Cyrano destabilizes miR-7-5p through TDMD (Kleaveland *et al*,
84 2018), while the circRNA CDR1as (also known as ciRS-7) yields a protection on miR-7-5p (Piwecka *et al*,
85 2017). We show that expression of an artificially linear version of *Cdr1as* triggers TDMD and is unable to
86 rescue the endogenous circRNA loss of function, suggesting that the circular topology of *Cdr1as* is

87 crucial for the evasion of TDMD. Finally, we show that certain circRNA-miRNA interactions might lead to
88 a phenomenon of miRNA stabilization, representing a potentially active mechanism during neuron-like
89 differentiation.
90

91 # Results

92 ## Artificial circRNA expression

93 In order to compare the effect of circular and linear RNAs on microRNA stability, we designed
94 constructs capable of expressing either linear transcripts or artificial circRNAs encompassing segments
95 of identical primary sequence (Figure 1A). Both the linear and circular RNAs contain 4 binding sites for
96 a candidate miRNA (miR-132) with proven TDMD-competent sequence complementarity (de la Mata *et*
97 *al*, 2015) (Figure EV1A). To express the circRNA, we followed a strategy consisting of inserting acceptor
98 and donor splice sites flanking the segment of the transcript to be circularized, plus Alu reverse
99 complementary sequences (RCS) from the introns of a naturally circularized RNA (human ZKSCAN1
100 exons 2 and 3 respectively), (Figure 1A) (Liang & Wilusz, 2014). In order to preferentially enrich the
101 expression of the circular over the linear variant in neurons, we introduced perfectly matched sites
102 against a highly expressed neuron-specific miRNA (miR-124) which are lost after RNA processing in the
103 backspliced circular product but remain present in the linear RNA isoform, thus rendering the linear –
104 but not the circular– RNA form susceptible to AGO2 slicing (Figure 1A). As a TDMD positive control, we
105 expressed a linear transcript with identical sequence to the circRNA-expressing construct, but lacking
106 the splice sites and the reverse complementary flanking introns that induce circularization (Liang &
107 Wilusz, 2014) (Figures 1A and EV1A). The latter constructs have been proved effective in triggering
108 TDMD in primary neurons (de la Mata *et al*, 2015). All constructs were packed into lentiviral vectors and
109 used to transduce mouse primary neurons.

110 To control the miRNA-mediated degradation of the linear byproduct, we generated two circRNA
111 expressing constructs, differing by seed-mutations in the miR-124 binding sites (Figure EV1A). We first
112 sought to validate that the constructs expressed a single circRNA species with covalently linked ends
113 and no concatemers or other spurious by-products, by performing Northern blot analysis of RNase R
114 treated or untreated samples from HEK293T cells –a cell line where miR-124 is not endogenously
115 expressed. We observed that both circRNA-expressing constructs bearing either perfect or seed-mutant

116 sites for miR-124, produced two bands: a single RNase R-resistant circRNA product and an RNase R-
117 sensitive linear RNA form. The fact that the artificial circRNA was not susceptible to the RNase R
118 digestion relative to the linear transcript, supports a circular structure (Figure EV1B and D). Importantly,
119 digital quantification of northern blot bands correlated strictly with the RT-qPCR measurements using
120 primers to amplify either the circular isoform exclusively (Figure 1A, primer pair #1) or both the linear
121 and circular isoforms combined –hereafter referred to as Total Output (TO)– (Figure 1A, primer pair #2),
122 further validating the latter method for subsequent analysis (Figure EV1C). Next, to rule out artifacts
123 that could be caused by template switching during cDNA synthesis and that could serve as templates
124 for the divergent primers -designed to amplify across the artificial circRNA backspliced junction- (Figure
125 1A, primer pair #1), we performed the PCR from cDNAs obtained with two different reverse
126 transcriptases (MMLV-RT & Superscript II). Amplification from both cDNAs produced identical PCR
127 products with identical sequences spanning the predicted backsplicing junction (Figure EV1E). Because
128 the two RT enzymes are unlikely to jump at the exact same sequences during a putative template
129 switching event, we conclude the transcripts produced from our expression system are bona fide
130 circRNAs.

131 In order to quantify the linear/circular RNA ratio produced by our circRNA-expressing constructs, the
132 relative intensities of the bands were acquired by densitometry using Image J. On average, the
133 linear/circular RNA ratio obtained was in the order of 4±1 in HEK293T cells (Figure EV1B), a cell line that
134 does not express miR-124 and therefore does not degrade the linear RNA. To validate that our strategy
135 was successful at expressing a circRNA while selectively degrading its counterpart linear transcript by
136 means of miR-124, we transduced the circRNA-expressing constructs into mouse primary neurons and
137 performed RT-qPCR using both the primers described above plus additional primers to amplify the
138 linear isoform exclusively (Figure 1A, primer pair #3). Remarkably, we observed that our strategy led to
139 a potent (3-4 fold) degradation of "leak" linear RNA without affecting circRNA abundance (Figure 1B).
140 Furthermore, circRNA levels produced from the circRNA-expressing construct were exceedingly higher
141 than from the construct expressing the linear RNA (TDMD inducer), with both constructs producing
142 equivalent total output levels (Figure 1C). Altogether, these results confirm that our system is effective
143 in expressing circRNAs while reducing the abundance of their cognate linear RNAs, making it a generally
144 useful tool in experiments aimed at dissecting circRNA function.

145

146 **CircRNA-expressing construct is incapable of triggering TDMD**

147 To explore whether linear and circular target topologies function differently to affect miRNA stability
148 through TDMD, we determined the extent to which a circular RNA topology can impact miRNA stability
149 via TDMD in neurons, a cell type known to display a potent TDMD effect (de la Mata *et al*, 2015). To this
150 end we transduced primary neurons with either linear or circRNA expression constructs bearing TDMD-
151 competent (bulged) or seed-mutant binding sites for miR-132, and measured miR-132 abundance by
152 an RT-qPCR Taqman assay. Whereas the linear TDMD inducer was capable of effectively destabilizing
153 miR-132, the circRNA-expressing construct showed no effect on miRNA stability. Considering that the
154 circRNA-expressing construct reduces the linear RNA abundance by 3-4 fold in neurons and that the TO
155 of the circRNA-expressing construct remains similar to that of the linear RNA-only expressing construct
156 (TDMD inducer), we conclude that: 1) the circRNA levels account for up to 30-50% of the total RNA
157 abundance expressed from the circRNA-expressing construct in neurons (compared to the ca. 25% in
158 HEK293T cells that lack endogenous miR-124), and 2) the fact that no miR-132 downregulation is
159 observed under these conditions suggests that up to the extent that we were able to express the
160 artificial circRNA, it appears unable to contribute to any additional TDMD effect, and it likely even
161 antagonizes the TDMD effect driven by its co-expressed linear counterpart. (Figures 1C and 2A). We
162 confirmed that miR-132 downregulation by the linear TDMD inducer was not a consequence of changes
163 in transcription and/or maturation of the targeted miRNA by showing that the abundance of the
164 primary transcript (pri-miR-132) and passenger strand (miR-132-5p) of miR-132 remained unchanged,
165 confirming that the reduction in the miR-132 guide strand was a bona fide post-transcriptional effect
166 occurring after miR-132 processing and therefore consistent with TDMD (Figure EV2A). To control for
167 the specificity of the linear TDMD inducer against miR-132, we measured the levels of four (4) additional
168 control mature miRNAs (miR-124, -128, -138 and -409). None of them were significantly affected,
169 confirming that the effect is indeed specific for miR-132 (Figure EV2A).

170 In order to determine whether the observed differential effect could be attributed to the inability of
171 the circular RNA to bind to the RISC complex, we set out an RNA immunoprecipitation experiment (RIP)
172 by specifically pulling-down AGO2 and isolating all copurifying RNA species. To this end, we co-
173 transfected HEK293T cells with FLAG/HA-AGO2 together with the different circRNA-expressing

174 constructs and a vector for pri-miR-132 (otherwise of low abundance in HEK293T cells) followed by
175 immunoprecipitation and RT-qPCR analysis. We observed that the artificial circRNA was effectively
176 pulled down together with AGO2 only when carrying bulged sites for miR-132 but not if the sites were
177 mutated at the miRNA seed-binding region (Figures 2B and EV2B-C). These results demonstrate that the
178 circular RNA is indeed able to specifically bind to the RISC complex, ruling out that defects in circRNA-
179 AGO2 binding could account for the observed lack of TDMD activity.

180 To exclude the possibility that the observed differences were a trivial consequence of an aberrant
181 localization of the circRNA relative to the linear isoform (Chen, 2020), we performed a purification of
182 nuclear and cytoplasmic subcellular fractions. Our results showed that the artificial circRNA accumulates
183 in the cytoplasm at similar proportions relative to the linear control and is only slightly lower in the
184 nuclear compartment (Figures 2C and EV2D-E), suggesting that the inability of the circRNA to trigger
185 TDMD is not related to it being retained in the nucleus.

186

187 Circular topology of *Cdr1as* is necessary to protect miR-7 from TDMD

188 To answer whether the inability to trigger TDMD was restricted to our circRNA expression system or
189 if it may actually be observed for other known endogenous circRNAs as well, we studied the case of the
190 *Cdr1as*-miR-7 interaction (Hansen *et al*, 2011, 2013; Memczak *et al*, 2013). To determine whether the
191 circular topology of *Cdr1as* has a role in modulating miR-7 abundance, we designed tools to manipulate
192 endogenous *Cdr1as* levels in rodent primary neurons (Fellmann *et al*, 2013). In order to knock down
193 *Cdr1as* we engineered a lentiviral vector to express a specific shRNAmiR (sh*Cdr1as*) (Figure EV3A) and
194 transduced it in primary neurons at high efficiency. Interestingly, the effective *Cdr1as* knockdown
195 achieved did not increase miR-7 levels as expected had *Cdr1as* been an active inducer of TDMD on this
196 miRNA. On the contrary, and in line with previous evidence (Piwecka *et al*, 2017), *Cdr1as* knockdown
197 reduced miR-7 levels, consistent with a stabilization role of the circRNA on this miRNA (Figure 3A-B).

198 To determine whether the observed effect was dependent on *Cdr1as*'s circular topology, we
199 attempted to rescue the *Cdr1as* knockdown with the expression of an artificial linear version of *Cdr1as*
200 –lin*Cdr1as*– lacking the sh*Cdr1as* target site. Interestingly, the drop of miR-7 abundance caused by the
201 knockdown of the endogenous *Cdr1as*, could be neither rescued nor enhanced by co-expressing the
202 linear *Cdr1as*, even though the artificial lin*Cdr1as* reached expressions levels similar to those of

203 endogenous *Cdr1as* in control cells (Figure 3A-B). Remarkably, expressing lin*Cdr1as* alone –without
204 knocking down endogenous *Cdr1as*– caused a significant destabilization of miR-7 (Figure 3C-D),
205 consistent with TDMD being driven by the RNA expressed under an artificial linear RNA topology.
206 Importantly, the linear lin*Cdr1as* did not induce a significant variation of the endogenous abundance of
207 (circular) *Cdr1as* (Figure EV3C). To exclude the possibility that miR-7 downregulation was a consequence
208 of changes in transcription and/or maturation of the targeted miRNA upon transduction of lin*Cdr1as*,
209 we measured the abundance of the primary transcript (pri-miR-7a-1), miR-7 passenger strands (miR-7a-
210 1-3p and miR-7a-2-3p) and two (2) additional control miRNAs (miR-9 and -132). Our result shows that
211 the guide strand miR-7-5p, but neither the passenger strands nor the other control miRNAs, undergo
212 degradation by the linear version of Cdr1as (Figure 3D, EV3D). This result confirms that the reduction in
213 the miR-7 is a post-transcriptional effect occurring after miRNA processing and is therefore compatible
214 with active TDMD triggered by the linCdr1as construct (EV3D). Careful inspection of the miR-7 sites
215 present in *Cdr1as* showed that no less than 3 of them indeed exhibit a base pairing complementarity
216 compatible with a TDMD-competent architecture (Figure EV3B) (Fuchs Wightman *et al*, 2018).
217 As an orthogonal strategy to reduce *Cdr1as* levels and rule out potential off target or indirect effects
218 caused by the sh*Cdr1as*, we used CRISPR/Cas9 genome editing to mutate the splicing sites of the
219 endogenous *Cdr1as* gene. To that end we expressed two sgRNAs against both donor and acceptor
220 splice sites of *Cdr1as* respectively (Figure EV3E). Despite an overall lower efficacy in *Cdr1as* knockdown
221 reached through CRISPR/Cas9 editing compared to the sh*Cdr1as*, we observed a similar effect
222 consistent with *Cdr1as* being unable to induce TDMD on miR-7 but rather leading to its stabilization
223 (Figure EV3E-G).
224 Overall, our results show that endogenous *Cdr1as* is unable to trigger TDMD on miR-7 but rather
225 stabilizes this miRNA. Accordingly, only if expressed as an artificially linear RNA can it engage in miR-7
226 degradation through TDMD, further supporting the notion that the natural circular/linear topology, and
227 not just the linear sequence of a RNA target, is a crucial determinant for engaging in such type of
228 regulation.
229

230 CircRNAs potentially stabilize dozens of microRNAs across neuron-like 231 differentiation

232 Based on our results, we hypothesized that circRNAs might possess the ability to influence miRNA
233 stability through evading TDMD and eventually protecting miRNAs from degradation. Yet, whether this
234 type of regulation could be a widespread phenomenon is unclear. To explore this possibility, we
235 analysed available sequencing data of miRNA, circRNA and mRNA expression from hESC H9 cells both
236 undifferentiated and differentiated into forebrain (FB) neuron progenitor cells (Chen *et al*, 2015; Zhang
237 *et al*, 2016). We reasoned that this model would be appropriate to test our hypothesis from the
238 viewpoint that a significant proportion of circRNAs are regulated along neuron differentiation –with
239 upregulation being more frequent than downregulation (You *et al*, 2015; Rybak-Wolf *et al*, 2015).
240 Concomitantly, neuron-specific miRNAs are known to become more susceptible to degradation in more
241 mature neurons (Krol *et al*, 2010), a scenario where circRNAs could act by selectively regulating miRNA
242 stability. In order to consider only the biochemically supported circRNA-miRNA pairs, we used the CLIP-
243 Seq experimentally supported mRNA-miRNA, lncRNA-miRNA and circRNA-miRNA interaction networks
244 catalogued in the STARBASE v3/ENCORI database (Yang *et al*, 2011; Li *et al*, 2014) as a proxy for bona
245 fide interactions.

246 We first followed a miRNA perspective approach aimed at analysing whether the abundance of
247 miRNAs across the neuron-like differentiation was dependent on the extent of "sponging" imposed by
248 circRNAs. To that end, we initially computed the total number of specific miRNA sites contributed by all
249 circRNAs weighed by circRNA levels before differentiation (hereafter referred to as "miRNA-specific
250 effective sites", see materials and methods and Dataset EV1). We observed that miRNA fold changes
251 across differentiation show no apparent correlation with the number of miRNA-specific effective sites
252 on all circRNAs (Figure 4A). In order to obtain a stoichiometrically relevant estimate of the "sponging
253 suffered" by each miRNA at the onset of differentiation, we further weighted the miRNA-specific
254 effective sites to each miRNA's abundance before differentiation (Figure 4B, ranked in Dataset EV1).
255 According to this analysis, the most highly "sponged" miRNAs, corresponding to those potentially
256 interacting with multiple and/or highly expressed circRNAs at higher circRNA:miRNA stoichiometries
257 early during differentiation, are significantly upregulated across differentiation relative to the least
258 "sponged" miRNAs (Figure 4B-C). We next searched for additional evidence in support of a stabilizing
259 effect of circRNAs which, by acting on top of transcriptional effects, could account for the observed
260 differences in mature miRNA fold changes between the different sponging quartiles. To that end we

261 estimated the change in pri-miRNA abundance as a proxy for change in transcription levels of the
262 respective miRNA genes across differentiation. Interestingly, while we observe a positive correlation
263 between mature miRNA and pri-miRNA fold changes, the correlation becomes weaker for the most
264 highly "sponged" than for the least "sponged" miRNAs (Figure 4D). By fitting the data to a multiple
265 regression model with interaction, we found that the fold change in mature miRNA levels for the more
266 highly sponged miRNAs (quartile "+++ sponged") seems differentially dependent on the fold change
267 of pri-miRNA levels relative to the least sponged miRNAs (quartile "- sponged") (i.e., the slope changes
268 by ≈2 fold, p-value for the interaction term = 0.0354) (Figure 4D). While this analysis shows that changes
269 in mature miRNA levels are to a large extent explained by changes in transcription of their host genes,
270 the impaired correlation and difference in slope observed for miRNAs in the most highly sponged
271 quartile are consistent with a stabilization effect that cannot be solely explained by changes in their
272 transcription rates. In sum, although we cannot rule out that the more highly upregulated miRNAs are
273 more efficiently processed from their pri-miRNAs than the less upregulated ones, our analysis argues
274 for a post-transcriptional effect of circRNAs on miRNA stability acting in parallel to –but independently
275 of– changes in miRNA transcription. This effect would occur through the concerted interaction of
276 individual miRNAs with multiple and/or highly expressed circRNAs across differentiation.

277 As a complementary approach from a circRNA perspective, we asked whether the extent of
278 "sponging capacity" offered by circRNAs, namely their ability to simultaneously interact with different
279 miRNAs across differentiation, could impact their own abundance. To that end we calculated a
280 "sponging capacity" index based on the total number of sites (for all miRNAs) present on each circRNA
281 weighed by circRNA levels before differentiation (see materials and methods and Dataset EV1).
282 Interestingly, we observed that an increasing "sponging capacity" index did not correlate with a visible
283 change in circRNA fold changes across differentiation, which is consistent with the notion that circRNAs
284 are not subjected to regulation by miRNAs (Figure 4E). The collection of miRNAs and circRNAs
285 interacting across this neuron-like differentiation might include more than a hundred miRNAs and
286 dozens of circRNAs. In fact, by focusing on the predicted most highly sponging circRNAs, this analysis
287 illustrates that circRNAs with the highest "sponging capacity" for miRNAs lie at highly connected nodes
288 within a complex network, further supporting the view that some individual circRNAs might act as
289 potential scaffolds for multiple miRNAs (Figure EV4A).

290

291 **Predicted binding of miRNAs to circRNAs through TDMD-like interactions**

292 In order to determine the existence of possible associations between specific features of circRNAs
293 and their ability to engage in potential miRNA-stabilizing interactions, we performed the following
294 analyses. We first compared the median length of circRNAs engaged in interactions with miRNAs
295 subjected to different degrees of sponging by circRNAs. We observed no association between the
296 circRNA median lengths and the degree of sponging (Figure EV4C). We next analysed the genomic
297 regions within transcripts that generate the circRNAs with predicted binding sites for miRNAs of
298 different sponging quartiles. Considering that most circRNAs are expressed from protein coding genes
299 (Guo *et al*, 2014), we analysed the overlapping genomic regions (CDS, 5'UTR, 3'UTR, etc) from such genes
300 only. We observed that the genomic region from which circRNAs originate does not correlate with the
301 degree of miRNA sponging they engage with across differentiation (Figure EV4D).

302 Our previous knowledge that a limiting number of bona fide TDMD sites –present even at sub-
303 stoichiometric levels– can act catalytically to outcompete the tens of thousands of miRNA binding sites
304 present in the transcriptome (de la Mata *et al*, 2015; Denzler *et al*, 2016; Kleaveland *et al*, 2018; Shi *et al*,
305 2020) might seem at odds with the interpretation arising from our results that those TDMD sites can be
306 nevertheless antagonized by a few thousand binding sites present on circRNAs. Conceivably, this
307 conundrum could be explained if the miRNA-stabilizing interactions involved sites on circRNAs with
308 TDMD-like architecture themselves. In this scenario, combined with their ability to avoid TDMD,
309 circRNAs bearing TDMD-like sites would act as more effective competitors against bona fide TDMD sites
310 than linear RNAs bearing canonical miRNA sites. To test this hypothesis, we searched for TDMD-like
311 architectures within both circRNAs and 3' UTRs of linear mRNAs using a TDMD-site prediction tool
312 (Soutschek *et al*, 2022). According to this analysis, the most highly "sponged" miRNAs are predicted to
313 interact through TDMD-like interactions with both linear and circRNA at a higher proportion than the
314 least sponged miRNAs, with the proportion of interactions involving circRNAs being overrepresented.
315 From this analysis we conclude that TDMD-like sites on circRNAs may be particularly effective in
316 competing for – and thus stabilizing– miRNAs across differentiation (Figure 5A-B and EV5).

317

318 **Discussion**

319 A long-lasting and largely unresolved question in the field is whether circRNAs' topology –i.e., their
320 circular nature– is intrinsically relevant for them to exert their molecular actions. Alternatively, the
321 circular form of some circRNAs might have been evolutionarily selected merely based on their
322 resistance to endonucleases that confer them special stability properties. Due to different technical
323 reasons, many of which are related to the expression systems employed, these key questions have not
324 been fully addressed so far.

325 While most experimental approaches have largely relied on knocking down or overexpressing
326 circRNAs in different organisms or cultured cells, undesirable artifacts can very commonly act as
327 confounding factors in the interpretation of the results. In particular, overexpression of circRNAs suffers
328 from a major caveat related to the unwanted linear RNA species that are inevitably co-expressed from
329 the commonly used expression vectors. This type of problem can easily lead to conclusions where
330 functions are wrongly assigned to circRNAs under circumstances where the associated linear transcripts
331 are the true functional molecules but are ignored in the experiments (Dodbele *et al*, 2021). We have
332 addressed this issue by designing a strategy that allows us to express circRNAs while keeping expression
333 of the counterpart linear product to a minimum. A similar strategy was previously reported in a different
334 context with the goal of restricting expression of transgenes to specific tissues (Brown *et al*, 2007). In
335 our hands the approach proved to work as an efficient tool to deliver high levels of circRNAs while
336 limiting the expression of the linear RNA derived from the circRNA construct (Figure 1).

337 We have exploited this tool to gain insight into the mechanism of the well-known role of circRNAs
338 in blocking miRNAs. Despite being neither prevalent nor unique to circRNAs as a class, the capacity to
339 inhibit or "sponge" miRNA silencing activity has been the most extensively documented function of
340 circRNAs (Chen, 2020; Dodbele *et al*, 2021). This abundance of papers likely obeys to historical reasons,
341 namely the fact that this was the first function to be reported for circRNAs since their rediscovery during
342 the last decade (Memczak *et al*, 2013; Hansen *et al*, 2013). In spite of this, a clear picture of the
343 mechanism by which some circRNAs act on miRNAs is still missing. For instance, it remains unclear
344 whether circRNAs act on miRNAs simply by blocking their function and/or by affecting their stability. In
345 this sense, although it has been speculated that circRNAs might trigger TDMD like linear RNAs, this
346 premise was never formally and experimentally tested so far (Gasparini *et al*, 2020). Our data suggest
347 the opposite: even when expressed at comparable levels, artificial circular RNAs of identical sequence

348 to those of TDMD-inducing linear RNAs, prove incapable of inducing TDMD (Figure 2). This is largely
349 recapitulated by the endogenous circRNA *Cdr1as* which cannot trigger TDMD on miR-7 –in fact it leads
350 to its stabilization as discussed below– unless artificially expressed as a linear RNA.

351 The fact that the protection of miR-7 exerted by *Cdr1as* was not recapitulated by our artificial circRNA
352 on miR-132, might be explained by the still partially present expression of the linear counterpart
353 containing TDMD-active miR-132 sites. An alternative explanation might be the emergent properties of
354 the *Cdr1as*-miR-7-Cyrano network. Based on the latter idea, the stabilization of miR-7 might emerge
355 from the inability of *Cdr1as* to drive TDMD in combination with its preserved ability to bind and compete
356 for miR-7, ultimately shielding the exceptionally potent TDMD activity driven by Cyrano on miR-7
357 (Kleaveland *et al*, 2018). A similar reasoning might apply to the fact that the artificial (linear) lin*Cdr1as*,
358 when expressed in combination with the knockdown of endogenous (circular) *Cdr1as*, does not
359 produce any additional reduction of miR-7 abundance: under these conditions, an unleashed Cyrano-
360 driven TDMD activity acting on miR-7 might reach a limit in miR-7 degradation rate which cannot be
361 further enhanced by an additional TDMD-competent target such as lin*Cdr1as* (Figure 3). In the presence
362 of *Cdr1as*, the system would be set to intermediate miR-7 degradation rates which could be further
363 enhanced by other TDMD-competent RNAs such as lin*Cdr1as* (see model in Appendix Figure S1).
364 Notably, a similar protection phenomenon has been observed in a prostate cancer cell line, where
365 knockdown of circ*CSNK1G3* bearing TDMD-like binding sites for miR-181b/d decreased their
366 abundance, while circ*CSNK1G3* overexpression increased it (Chen *et al*, 2019) (Figure S2F).

367 The molecular basis explaining the functional differences between circRNAs and their cognate linear
368 transcripts in triggering TDMD, might obey to the structural properties affected by the circular-linear
369 topology. Based on a previous report, whereas circRNAs inhibit PKR-mediated innate immune
370 responses, their cognate linear counterpart transcripts cannot. The explanation behind this
371 phenomenon seems to be the inherent ability of circRNAs to fold into more stable short local secondary
372 structures compared to their linear counterpart transcripts. This in turn seems to lead to a more stable
373 interaction between circRNAs and PKR (Liu *et al*, 2019). Based on similar principles –but with an opposite
374 outcome– the greater tendency of circRNAs to form secondary structures could confer them an extra
375 rigidity that could ultimately limit their capacity to drive TDMD. This seems in agreement with previous
376 reports showing that an extended miRNA:target basepairing *per se* is not enough to trigger TDMD:

377 miRNA binding must also occur within a conformationally flexible region of the target for TDMD to be
378 active (Pawlica *et al*, 2016; Li *et al*, 2021; Fuchs Wightman *et al*, 2018). In line with this idea, two in-depth
379 studies have contributed to our understanding of TDMD by pinpointing the ubiquitin ligase ZSWIM8 as
380 a mediator of the mechanism (Shi *et al*, 2020; Han *et al*, 2020). These findings showed that the binding
381 of TDMD-competent target RNAs drives a conformation change on AGO proteins (loaded with specific
382 miRNAs) that leads to their poly-ubiquitination and degradation, leaving the specific miRNAs
383 unprotected and susceptible to degradation by general nucleases. The extra rigidity of circRNAs could
384 preclude the conformational change of AGO, thus bypassing TDMD while remaining bound to the RISC
385 complex. A recent report might be consistent with this view by showing differences between the
386 thermodynamic properties of linear and circular RNA in binding to complementary short RNAs,
387 favouring a model where circRNAs might bind to miRNAs more efficiently than their cognate linear
388 RNAs (Petkovic *et al*, 2021).

389 An alternative explanation could relate to the differential ability of distinct RNA species in recruiting
390 TDMD machinery factors such as ZSWIM8. In that sense, several characteristics of circRNAs could be
391 critical, such as their lack of capping and poly-A tails. However, the latter seems dispensable for TDMD
392 based on the fact that HSUR-1, which lacks a poly-A tail, effectively drives TDMD on miR-27 (Cazalla *et*
393 *al*, 2010; Pawlica *et al*, 2016). Additionally, specific sequence elements within transcripts are required for
394 TDMD. For instance, both the miR-7 and miR-17 binding sites that exist within known TDMD-inducing
395 targets (Cyrano and HCMV's UL144-145 respectively), depend on sequences that are located outside of
396 the miRNA site *per se* for efficiently triggering of TDMD (Lee *et al*, 2013; Kleaveland *et al*, 2018; Han *et al*,
397 2020). Such sequences might be absent or simply occluded within the more highly structured circRNAs,
398 possibly explaining their observed inability to drive TDMD.

399 Interactions between miRNAs and competing-endogenous RNAs (ceRNAs) have received a broad
400 attention in the recent years as they might represent a mechanism of miRNA inhibition (Tay *et al*, 2014).
401 However, due to stoichiometry considerations, the likelihood that individual ceRNAs titrate the total
402 amount of miRNA available for target repression seems limited (Denzler *et al*, 2014; Jens & Rajewsky,
403 2015; Bosson *et al*, 2014; Pinzón *et al*, 2017; Denzler *et al*, 2016). Instead, models where multiple ceRNAs
404 regulate single miRNAs have been favoured (Ameres & Zamore, 2013; Dodbele *et al*, 2021). The case of
405 *Cdr1as*-miR-7 pair might represent an outstanding example functioning in an analogous way: *Cdr1as* is

406 a highly expressed circRNA with > 60 evolutionarily conserved miR-7 binding sites based on previous
407 reports (Memczak *et al*, 2013; Hansen *et al*, 2013) (67 predicted sites for miR-7 in humans based on the
408 STARBASE/ENCORI database), significantly exceeding the average number of sites annotated for
409 circRNAs (based on Starbase/ENCORI database, see Dataset EV2). On the other hand, while *Cdr1as* is
410 highly expressed in human, rat and mouse brain, miR-7 tends to display medium to low expression. Our
411 results favour a model where the concerted interaction of multiple circRNAs with individual miRNAs
412 seems the most likely and relevant scenario in regulating miRNA stability. Interestingly, among the
413 miRNAs that are upregulated upon ZSWIM8 knockdown in mouse induced neurons (Shi *et al*, 2020), two
414 belong to the most highly "sponged" miRNAs according to our analysis (miR-7 and also miR-409-3p),
415 suggesting that such type of regulation might be acting in neuron differentiation and possibly in
416 pathophysiological conditions (Figure EV4B).

417 An increasing number of TDMD natural examples have arisen in the past few years, including both
418 endogenous and viral transcripts (Ameres *et al*, 2010; Cazalla *et al*, 2010; Bitetti *et al*, 2018; Ghini *et al*,
419 2018; Li *et al*, 2021; Simeone *et al*, 2022; Kingston *et al*, 2022). Furthermore, the discovery that TDMD is
420 more widespread than initially thought suggests that more examples will be discovered (Shi *et al*, 2020;
421 Han *et al*, 2020). In this scenario, circRNAs' capacity to evade such regulation could confer them an
422 advantage in regulating miRNA stability even (or especially) when involving highly complementary
423 pairing architectures that would otherwise drive TDMD in the context of linear RNAs. Our findings
424 suggesting that the most highly "sponged" miRNAs seem to engage in TDMD-like interactions with
425 circRNAs more frequently than the least "sponged" miRNAs seems in line with this idea. Although we
426 ignore the extent to which circularization may affect the thermodynamic and/or kinetic properties of
427 miRNA-target pairing, we speculate that, by avoiding TDMD, sites with TDMD-like architectures within
428 circRNAs might provide an enhanced stability and/or decreased dissociation rate relative to sites with
429 canonical architectures present within the more abundant linear transcripts. Accordingly, by binding
430 and sequestering miRNAs through TDMD-like architectures, certain combinations of circRNAs might
431 stabilize specific miRNAs, rendering them unavailable for TDMD even when expressed at an overall sub-
432 stoichiometric level relative to the whole set of linear targets present in the cell. This type of regulation
433 would in turn be compatible with a potential reversibility of circRNA's inhibitory function on miRNAs.

434 A complex and yet unresolved aspect of the role of circRNAs in regulating miRNAs relates to our
435 inability to predict their outcome on canonical miRNA silencing activity. In this sense, depending on
436 factors such as the relative binding site architectures and the relative stoichiometries of the molecules
437 involved, different outcomes may be expected. For instance, miRNA stabilization by circRNAs could lead
438 to greater average target repression due to increased abundance of the cognate miRNAs. This is
439 consistent with the effect that we observe in primary neurons upon *Cdr1as* KD (Appendix Figure S2B)
440 and with previously published analysis in mouse cortex upon *CDR1as* knockout (Piwecka *et al*, 2017),
441 where miR-7 predicted targets are significantly upregulated upon *CDR1as* knockout. However, miRNA
442 stabilization by circRNAs could alternatively be accompanied by an overall tight blockade of miRNA
443 silencing activity, leading to the opposite outcome in such contexts. Accordingly, our reanalysis of the
444 data from a prostate cancer model (Chen *et al*, 2019) shows that a decrease of miR-181b/d upon
445 circ*CSNK1G3* knockdown (analogous the case of miR-7 and *Cdr1as*) leads to an overall downregulation
446 of miR-181b/d predicted targets. Our side-by-side reanalysis of both datasets from these reports
447 suggests an overall opposite effect of specific miRNA stabilization by circRNAs on target silencing in
448 these different cellular contexts (Appendix Figures S2B-E). Based on this, a direct correlation between
449 the eventual stabilization of miRNAs by circRNAs and their ensuing downstream effect on miRNA
450 canonical silencing cannot be currently established, highlighting the need of further dissecting the role
451 of circRNAs on miRNA target repression. Eventually, more in-depth knowledge of the players involved,
452 their relative stoichiometries and dynamics will help us understand the emergent properties arising
453 from different systems and the full potential and adaptive value of circRNAs in miRNA regulation.

454

455 ## Limitations of the study

456 In this study we have generated a vector capable of expressing a circRNA with reduced levels of the
457 linear "leak" RNA that is otherwise inevitably produced from these kinds of constructs. As shown in this
458 work, although the principle works in our hands, the net circRNA-to-linear RNA relative expression yield
459 that we obtain is still suboptimal. Bearing this limitation in mind, our data support the notion that the
460 circRNA levels that we achieve are enough to prevent TDMD, either by not contributing to any
461 additional TDMD effect and/or by antagonizing the TDMD driven by its co-expressed linear counterpart.

462 We are aware that effectively expressing circRNAs from artificial vectors is a general debate in the field,
463 and we hope that our efforts to generate an improved system for circRNA expression might contribute
464 to the development of even better strategies in the future.

465 It is important to stress the idea that additional properties of different circRNAs might determine
466 their ability to bypass TDMD, including but not limited to circRNA modifications (RNA methylation, etc)
467 and specific secondary structures, none of which have been systematically addressed in our work. More
468 studies will be required to determine whether the avoidance of TDMD by circRNAs in particular and the
469 ensuing miRNA stabilization in general, is a widespread phenomenon.

470 Furthermore, we have shown that a group of miRNAs sharing high "availability" of sites on circRNAs
471 relative to their own abundance (defined above as "sponging suffered" coefficient) is preferably
472 upregulated across a neuron-like differentiation. It is worth emphasizing that this correlation does not
473 imply causality and that functional experiments will be needed in the future in order to validate this
474 possibility. Finally, the enrichment of TDMD-like sites that we report in this study is based solely on
475 predicted –though not experimentally validated– sites using the scanMiR bioinformatic tool (Soutschek
476 *et al*, 2022).

477

478 # Materials and methods

479 ## Plasmid construction

480 Unless otherwise specified, the lentiviral vectors are based on pRRLSIN.cPPT.SYN.WPRE (de la Mata
481 *et al*, 2015).

482 Linear *Cdr1as* (lin*Cdr1as*) was amplified by PCR from rat genomic DNA (see primers at Table EV1).
483 Following gel purification (QIAquick Gel Extraction Kit), and cloning into pCR II-Blunt-TOPO
484 (ThermoFisher) it was then subcloned into pRRLSIN.cPPT.SYN.WPRE. The linear *Cdr1as* version lacking
485 the sh*Cdr1as* target site –lin*Cdr1as*$^{671-}$ was generated by PCR amplification of a *Cdr1as* fragment lacking
486 a 174-bp 3'-terminal segment that encompasses the miR-671 binding site, and re-cloning it into the
487 original backbone's BamHI-SalI sites (Table EV1). The linear transcript used as a negative control consists
488 of GFP expressed from pRRLSIN.cPPT.PGK-GFP.WPRE (Addgene plasmid 12252).

489 The pri-miR-132 and pri-miR-124 expressing constructs were made by amplifying the pri-miRNA
490 fragments (Table EV1) from miRNASelectTM pEGP-mmu-mirna expression vectors (Cell Biolabs) and
491 subsequently cloning them into the BamHI-BsrGI sites of pRRLSIN.cPPT.SYN.WPRE.

492 The shRNAmiR (sh*Cdr1as*) is an engineered version miR-671 –previously described as a natural
493 *Cdr1as* regulator (Piwecka *et al*, 2017; Kleaveland *et al*, 2018)– designed to be fully complementary to
494 the circRNA and maximizing its slicing capacity (Figure EV3A). The sh*Cdr1as* lentiviral vector was
495 constructed by replacing the pri-miRNA fragments from the previously described vectors using BamHI-
496 NheI (Table EV1), and inserting a synthetic DNA (gBlock gene fragment, IDT) by Gibson Assembly
497 (Gibson *et al*, 2009).

498 CircRNA-expressing constructs were constructed inserting gBlocks (Integrated DNA Technologies)
499 encompassing the ZKSCAN1 upstream and downstream introns (Liang & Wilusz, 2014) flanking
500 mCherry and bulged or seed-mutant miR-132 sites (de la Mata *et al*, 2015) downstream of a Tetracyclin-
501 inducible promoter (TREp, see Figure 1A and Table EV1). Perfect or seed-mutant sites for miR-124 were
502 subsequently inserted downstream or the circularizable region (Figure EV1A). Linear TDMD inducers
503 expressing mCherry upstream of bulged or seed-mutant miR-132 sites were previously described (de la
504 Mata *et al*, 2015).

505 The lentiviral vector driving expression of FLAG/HA-AGO2 (human) from the Syn promoter (pLV-
506 FLAG-HA_AGO2) was generated by amplifying FLAG/HA-AGO2 from pIRESneo-FLAG/HA AGO2
507 (Addgene plasmid 10822).

508 The construct for CRISPR/Cas9 genome editing of *Cdr1as* splicing sites is based on lentiCRISPRv2
509 (Addgene plasmid 52961), following the Zhang Lab protocol (Sanjana *et al*, 2014; Shalem *et al*, 2014)
510 (Primers in Table EV1).

511

512 HEK293T culture and transient transfection

513 HEK293T cells were available in our institute. Cells were tested for mycoplasma contamination and
514 only clean stocks were further used for our experiments. Cells were grown in DMEM-F12 (Gibco)
515 supplemented with 10% (v/v) FCS and 25 U/mL Penicillin-Streptomycin (Gibco) and were plated for
516 transfection at 100,000 cells/well on 24-well plates. One day after plating, cells were transfected using
517 the PEI method as previously described (de la Mata *et al*, 2015).

518

519 ## Lentivirus production and transduction

520 Recombinant lentiviral particles were produced in HEK293T cell line. Cells were co-transfected using
521 the PEI method with the lentiviral expression vector and two 2nd generation lentiviral packaging
522 vectors: pMD2.G expressing the VSV-G envelope gene (Addgene plasmid 12259) and pCMVR8.74
523 expressing the gag/pol genes (Addgene plasmid 22036). The supernatants containing the viral particles
524 were collected 48–72 h after transfection, concentrated using centrifugal filter units (Amicon Ultra-15,
525 molecular weight cutoff 100 kDa, Millipore Cat. #UFC910024) as further checked as previously described
526 (de la Mata *et al*, 2015).

527

528 ## Animals used in this study

529 All animal tissues used in this study were obtained under experiment protocol no. No.2020-04-DR
530 with the approval from the Comisión Institucional para el Cuidado y Uso de los Animales de Laboratorio
531 (CICUAL) at the Instituto de Investigación en Biomedicina de Buenos Aires (IBioBA) – CONICET – Partner
532 Institute of the Max Planck Society.

533

534 ## Neuronal cultures and lentiviral transduction

535 Cortical and hippocampal neurons were dissected from embryonic day 16.5 and 18.5 (E16.5 and
536 E18.5) respectively CD1 embryos of mixed sex. Culture preparation was performed as previously
537 described (Giusti *et al*, 2014; Vogl *et al*, 2015). Briefly, cortex from CD1 mouse embryos were dissected
538 and a neuronal suspension was prepared through Trypsin digestion and mechanical disruption of the
539 tissue. Neurons were plated in 24 multi-well plates at a density of 80cells/mm2 (150.000 cells per well)
540 and maintained in Neurobasal-A media (ThermoFisher) with 2% B27 and 0.5 mMGlutaMAX-I
541 (ThermoFisher) at 37 °C and 5% CO2. CD1 mice for neuronal cultures were provided by our Specific
542 Pathogen Free Animal Facility.

543 The euthanasia of the animals to generate primary neuronal cultures was performed under
544 experiment protocol no. 2020-04-DR which was evaluated by the Institutional Animal Care and Use
545 Committee of the IBioBA-CONICET according to the Principles for Biomedical Research involving

546 animals of the Council for International Organizations for Medical Sciences and provisions stated in the
547 Guide for the Care and Use of Laboratory Animals.
548 Neurons were transduced 4-7 days after plating (DIV4-7) with lentiviral constructs: lin*Cdr1as*$^{671-}$,
549 sh*Cdr1as*, the linear control or a combination of these, appropriately described in Results and Figures.
550 The vectors driving each of the circRNA-expressing constructs were transduced in combination with a
551 lentiviral construct expressing the tetracycline-controlled transactivator protein (LV-Syn-tTA). RNA was
552 extracted at DIV11 as indicated below.
553

554 **FLAG/HA-AGO2 transfection and immunoprecipitation (AGO2 RIP)**

555 The FLAG/HA-AGO2 expressing plasmid was transfected into HEK293T cells as described above.
556 Immunoprecipitation of FLAG/HA-AGO2 was performed with Anti-FLAG M2 Magnetic Beads (Sigma.
557 Cat # M8823). Beads were washed twice with TBS buffer (50 mM Tris HCl, 150 mM NaCl, pH 7.4). For each
558 immunoprecipitation (IP), one 6-cm plate with 50% confluency was used. Cells were washed once with
559 cold PBS and lyzed in 500 µl of lysis buffer [50 mM Tris–HCl pH 7.5, 150mM NaCl, 1% (v/v) TRITON X-100,
560 1 mM EDTA, containing protease inhibitors (cOmplete, EDTA-free Protease Inhibitor Cocktail, Roche)
561 and RNase inhibitor (Invitrogen)]. The lysates were incubated 30 minutes on ice, cleared by
562 centrifugation at 16,000 g for 10 minutes at 4 degrees and mixed with the washed beads. After 2 hours
563 of rotation at 4 degrees, the beads were washed three times with TBS buffer. As a control for the IPs,
564 non-transfected HEK293T cells were used. FLAG/HA-AGO2 expression and immunoprecipitation
565 efficiency were determined by Western blot using anti-HA antibody (clone 3F10, Roche). RNA was
566 extracted by adding Trizol reagent (Invitrogen) directly on the beads.
567

568 **Subcellular fractionation**

569 Briefly, the circRNA-expressing construct and the linear control were transfected into HEK293T cells
570 as described above, in 6-well plates at 50% confluency. After 48 hours, cells were harvested using 500
571 ⊠l of PBS, transferred to a microcentrifuge tube and centrifuged at 500 g for 5 minutes. The supernatant
572 was discarded, and the pellet resuspended in 350 ⊠l of PBS plus 0.1% NP-40 (IGEPAL). 150 ⊠⊠l were
573 separated and called TOTAL fraction. The remaining volume was centrifuged for 10 seconds at 10,000
574 rpm. 150 ⊠l of the supernatant were separated and called CYTOPLASM fraction. The pellet was

575 resuspended in 150 µl of PBS plus 0.1% NP-40 (IGEPAL) and centrifuged again at 10,000 rpm. The
576 supernatant was discarded, and the pellet resuspended in 150 µl of PBS plus 0.1% NP-40 (IGEPAL). This
577 was called the NUCLEAR fraction.
578 Out of the 150 µl of each fraction, 75 µl were used for Western Blotting and 75 µl for RNA
579 extraction followed by reverse transcription and quantitative polymerase chain reaction (RT-qPCR).
580

581 **RNA extraction**

582 Total RNA extractions were made using Trizol reagent (Invitrogen) following the manufacturer's
583 instructions.
584

585 **RT-qPCR quantification**

586 MiRNA and *U6* expression levels were determined by using Taqman® microRNA Assays (Applied
587 Biosystems) following the manufacturer's instructions or using SYBR Green and step-loop RT-qPCR (see
588 Table EV3 for oligo design). MicroRNA levels were normalized to *U6* RNA levels. Standard curves for the
589 analysed miRNAs and *U6* RNA were performed with serial dilutions of selected cDNAs, allowing
590 calculation of relative abundances. For quantification of target mRNAs, the artificial circRNA and *Cdr1as*,
591 total RNA was treated with RNase-free Dnase I (DNA-freeTM Kit, Ambion) and reverse transcribed using
592 random hexamers and SuperScriptTM II Reverse Transcriptase (Invitrogen) or MMLV-RT (Sigma),
593 following the manufacturer's instructions. The abundance of target mRNAs, artificial circRNA and *Cdr1as*
594 were determined by SYBR green qPCR using a custom-made qPCR mix (Table EV2) and specific primers
595 (detailed at Table EV3). Alternatively, INBIO highway qPCR SYBR green mix was used (Ref M130).
596 Standard curves for the analysed amplicons were performed with serial dilutions of selected cDNAs,
597 allowing calculation of relative abundances.
598

599 **Northern blot analysis**

600 Northern blot analysis was performed according to standard procedures (Roditi *et al*, 1987). A total
601 amount of 10 µg of RNA was loaded in each lane. The radioactively labelled probe, corresponding to
602 the mCherry CDS fragment, was prepared using the Megaprime DNA labelling kit (Amersham
603 Biosciences) according to manufacturer's instructions. The 18S RNA from the agarose gel run was used

604 as loading control. Blots were hybridized at 65° and washed in 0.2× SSC/0.1% SDS. The blots were
605 exposed to Phosphorimager screens and scanned with Typhoon FLA 7000 (GE Healthcare Life Sciences).
606 The relative intensities of the bands were measured by densitometry using ImageJ.
607

608 **Western blot analysis**

609 Protein samples were separated on 12% SDS-polyacrylamide gels and transferred to PVDF
610 membranes. Membranes were incubated with primary antibodies: anti-HA 3F10 (Rat, 1:2500), anti-
611 Tubulin (polyclonal rabbit anti β Tubulin H-235 from Santa Cruz Biotechnology, 1:2500) and Histone-3
612 (polyclonal rabbit anti H3 H-0164 from Merk, 1:2500). After washing, membranes were incubated with
613 IRDye® 800CW (LI- COR Biosciences) secondary antibodies. Bound antibody was detected an Odyssey
614 imaging system (LI-COR Biosciences).
615

616 **Statistical analysis**

617 R programming language was used to process information, visualize and design graphs, and
618 perform statistical tests. Data was normalized and scaled across experiments using Unit Length
619 Normalization. Bar, line, scatter, dot and boxplots were designed using the ggplot2 (Wickham, 2016)
620 and ggpubr packages. Statistical tests were done using base R and/or ggpubr (and its complement
621 rstatix) (https://rpkgs.datanovia.com/ggpubr/index.html). For experiments where two conditions were
622 compared, we performed unpaired t-tests, and for those where multiple comparisons were made, we
623 used the Bonferroni correction (ns: $p > 0.05$, *: $p <= 0.05$, **: $p <= 0.01$, ***: $p <= 0.001$, ****: $p <= 0.0001$).
624 For comparisons involving multiple groups we used either ANOVA followed by Tukey multiple
625 comparisons, Generalized Linear Models (GLM) with emmeans (https://github.com/rvlenth/emmeans),
626 or Wilcoxon rank sum test p-values (corrected with the Hochberg method for multiple comparisons) as
627 indicated in the text. When comparing several miR-7 targets across conditions, we performed a two-
628 way ANOVA followed by Tukey multiple comparisons, showing the adjusted p-value.
629

630 **Bioinformatic analysis of circRNA-miRNA interactions**

631 Two publicly available datasets produced by the Chen Lab were combined to generate a
632 comprehensive analysis taking into account miRNA, circRNA and mRNA expression during

633 differentiation of H9 (hESC) cells to H9 forebrain neurons. From GEO Accession GSE73325 (Zhang *et al*,
634 2016) we obtained data for circRNA and mRNA expression. From GEO Accessions GSE56152 and
635 GSE63709 (Chen *et al*, 2015) we obtained data for microRNA expression. Noteworthy, although the
636 same procedure for differentiation was followed (Zhang *et al*, 2016; Chen *et al*, 2015), sequencing was
637 done on different days (D26 and D35, respectively). We realize this is suboptimal, nevertheless we
638 proceeded with the analysis considering this the best data available to approach our questions.

639 Data of the interactions between circRNAs and miRNAs was retrieved from Starbase/ENCORI v3
640 database (http://starbase.sysu.edu.cn; (Yang *et al*, 2011; Li *et al*, 2014)). This particular source was
641 selected because it combines site prediction by several programs with experimental validation (e.g., by
642 CLIP). The main parameters chosen for downloading through their API were: assembly = hg19,
643 geneType= circRNA & miRNA, clipExpNum=1, program= all, programNum= 2, target= all and cellType=
644 all.

645 A condensed spreadsheet summarizing all the previously mentioned data can be found at Dataset
646 EV3.

647 The analysis was done in R, briefly:

648 • The expression tables were loaded and merged using the Tidyverse package (Wickham *et al*, 2019)
649 and/or the readxl package (Wickham & Bryan, 2022), while the circRNA-miRNA interactions table
650 was joined using the Fuzzyjoin package (https://CRAN.R-project.org/package=fuzzyjoin) to
651 consider genomic locations of both the circRNAs and the miRNA sites.
652 • Log_2 fold changes across differentiation were calculated for each type of RNA.
653

654 Analysis from a miRNA perspective:

655 • An absolute number of validated miRNA-specific sites on every circRNA (when present) was
656 calculated.
657 • A relative number of effective miRNA-specific sites was calculated by weighing the above number
658 (i.e. the absolute number of miRNA-specific sites on every circRNA) to the number of backspliced
659 junction reads as an estimate of the contribution of each circRNA.
660 • A total number of effective sites was calculated per miRNA (referred to as "miRNA-specific effective
661 sites" later on) by summing all the effective miRNA-specific sites among all circRNAs,.

662 • A coefficient of "sponging suffered" by each miRNA was defined by dividing the above number
663 ("miRNA-specific effective sites") by the miRNA abundance pre-differentiation. To simplify the
664 analysis, we separated miRNAs in quartiles of increasing sponging suffered coefficients and
665 performed the downstream analysis based on them.
666
667 Analysis from a circRNA perspective:
668 • The sum of all (i.e. pooling all miRNAs) absolute numbers of validated miRNA sites on each circRNA
669 (when present) was calculated.
670 • The "sponging capacity" index for each circRNA was calculated by multiplying the above number
671 to the number of junction reads pre-differentiation.
672
673 All graphs were programmed and illustrated using the packages ggplot2 (Wickham, 2016), ggrepel
674 (https://CRAN.R-project.org/package=ggrepel) and/or viridis (https://CRAN.R-
675 project.org/package=viridis). The network diagram (Figure EV4A) was done using IGraph package
676 (https://igraph.org/r/). Statistical analysis of the boxplots was done and added to the graphs using
677 ggpubr (https://rpkgs.datanovia.com/ggpubr/index.html).
678 For pri-miRNA analysis we used the Galaxy platform (The Galaxy platform for accessible,
679 reproducible and collaborative biomedical analyses: 2022 update., 2022). Briefly, raw reads extracted
680 from GSE73325 were trimmed using Trim Galore! (https://github.com/FelixKrueger/TrimGalore) and
681 mapped to the human reference genome (hg38) with the RNA-STAR aligner (Dobin *et al*, 2013). Pri-miR
682 counts were obtained from the mapped BAM files using featureCounts (Liao *et al*, 2014) and the
683 annotation file (has.gff3) retrieved from miRBase (Kozomara *et al*, 2019).
684

685 **Bioinformatic prediction of TDMD-like sites on circRNAs**

686 To predict TDMD-like sites on circRNAs, we used the scanMiR package (Soutschek *et al*, 2022). Briefly,
687 all reported human circRNA sequences were retrieved from circBase (Glažar *et al*, 2014) and used as an
688 input for the *findSeedMatches* function from scanMiR to predict TDMD-like sites for every miRNA
689 present. The data was filtered to keep only those sites on circRNAs that had at least one junction read
690 in the neuron-like differentiation data (see above). Finally, we calculated the proportion of miRNAs with

691 predicted TDMD-like sites (computed as those with at least one TDMD-like site on circRNAs/linear RNAs)
692 within each of the quartiles of increasing "sponging suffered" coefficients. Fisher's Exact tests between
693 each quartile and the least "sponged" quartile ("- sponged") were performed to assess enrichment. The
694 ggpie and rstatix packages were used to generate the pie charts and the ggpubr package to do the
695 violin plot and t-tests.

696

697 **Bioinformatic analysis of miR-7 and miR-181b/d targets**

698 Targets for miR-7 were retrieved from TargetScan 7.1 mouse (Agarwal *et al*, 2015) while the ones for
699 miR-181b/d from TargetScan 7.2 human (Agarwal *et al*, 2015). Raw RNA-seq counts were downloaded
700 for *Cdr1as* KO data (Piwecka *et al*, 2017) and circCSNK1G3 KD (Chen *et al*, 2019), accessions GSE93130
701 and GSE113124, respectively. A differential expression analysis was performed using the DESeq2
702 package (Love *et al*, 2014). Graphs were made using the results of the analysis and the packages
703 mentioned above.

704

705 Data availability

706 This study did not produce novel next generation sequencing datasets. Scripts and functions used
707 to produce the results and plots shown in this paper can be found at:
708 https://github.com/mmataLab/ciR-miR-stability

709

710 Acknowledgements

711 We thank Isabel Roditi for providing materials and discussing experiments, Helge Grosshans, Alberto
712 R. Kornblihtt, Jeremy Wilusz and Javier Cáceres for a critical reading of the manuscript, Pierre-Luc
713 Germain for a critical reading and general discussion of the manuscript, Valeria Buggiano for technical
714 assistance and Luciana Giono for creating figure illustrations. M.d.I.M. is funded by grants from Agencia
715 Nacional de Promocion Cientifica y Tecnológica (ANPCyT) of Argentina (PICT- 2016-0499 and PICT-2018-
716 0478_PRH 2016-0002). D.R. acknowledges the support of the Volkswagen, Stiftung, the Max Planck
717 Society, the Fondo para la Convergencia Estructural de Mercosur (COF 03/11), the Agencia Nacional de

Promoción Científica y Tecnológica (ANPCyT) of Argentina (PICT- 2019-0499 and PICT-PRH 2014-3782) and the Ministerio de Ciencia, Tecnología e Innovación Productiva of Argentina (MinCyT-BMBF AL15/10). J.P.F. is funded by grants from Ministerio de Ciencia, Tecnología e Innovación Productiva of Argentina (MINCyT) (BMBF/MINCYT MIGRAMIRNA Al/17/05), Agencia Nacional de Promocion Cientifica y Tecnologica (ANPCyT) of Argentina (PICT-2017-2401, PCE-GSK-2017-0052), Glaxo-SmithKline (PCE-GSK-2017-0052) and Fundación Progreso de la Medicina (GF N03/2017).

Author contributions

D.R. and M.d.l.M. conceived the project and designed and interpreted the experiments. F.F.W. and J.L. designed, performed and interpreted most of the experiments. F.F.W. conceived, performed and interpreted most of the computational analysis. M.d.l.M. conceived, performed and interpreted some of the computational analysis. G.S. and M.S. contributed with the use of the scanMiR package to obtain the TDMD-like site enrichment results and discussed strategies for data analysis. J.L. and S.G. handled animals and prepared the neuron primary cultures. L.B. performed the subcellular fractionation experiments. B.P. performed the Northern blot analysis. P.G. performed the subcloning of some of the constructs used in the study. J.P.F. designed some of the experiments and discussed experimental strategies. D.R. and M.d.l.M. co-supervised the whole project. The manuscript was written by F.F.W., D.R. and M.d.l.M.

Conflict of interest

The authors declare that they have no conflict of interest.

739 # References

740 Agarwal V, Bell GW, Nam JW & Bartel DP (2015) Predicting effective microRNA target sites in mammalian
741 mRNAs. *eLife* 4: 1–38

742 Ameres SL, Horwich MD, Hung J-H, Xu J, Ghildiyal M, Weng Z & Zamore PD (2010) Target RNA-directed
743 trimming and tailing of small silencing RNAs. *Science* 328: 1534–1539

744 Ameres SL & Zamore PD (2013) Diversifying microRNA sequence and function. *Nat Rev Mol Cell Biol* 14:
745 475–488

746 Bartel DP (2018) Metazoan MicroRNAs. *Cell* 173: 20–51

747 Bitetti A, Mallory AC, Golini E, Carrieri C, Carreño Gutiérrez H, Perlas E, Pérez-Rico YA, Tocchini-Valentini
748 GP, Enright AJ, Norton WHJ, *et al* (2018) MicroRNA degradation by a conserved target RNA
749 regulates animal behavior. *Nat Struct Mol Biol* 25: 244–251

750 Bosson AD, Zamudio JR & Sharp PA (2014) Endogenous miRNA and target concentrations determine
751 susceptibility to potential ceRNA competition. *Mol Cell* 56: 347–359

752 Brown BD, Gentner B, Cantore A, Colleoni S, Amendola M, Zingale A, Baccarini A, Lazzari G, Galli C &
753 Naldini L (2007) Endogenous microRNA can be broadly exploited to regulate transgene
754 expression according to tissue, lineage and differentiation state. *Nat Biotechnol* 25: 1457–1467

755 Cazalla D, Yario T & Steitz JA (2010) Down-regulation of a host microRNA by a Herpesvirus saimiri
756 noncoding RNA. *Science* 328: 1563–1566

757 Chen L-L (2020) The expanding regulatory mechanisms and cellular functions of circular RNAs. *Nat Rev*
758 *Mol Cell Biol* 21: 475–490

759 Chen S, Huang V, Xu X, Livingstone J, Soares F, Jeon J, Zeng Y, Hua JT, Petricca J, Guo H, *et al* (2019)
760 Widespread and Functional RNA Circularization in Localized Prostate Cancer. *Cell* 176: 831-
761 843.e22

762 Chen T, Xiang J-F, Zhu S, Chen S, Yin Q-F, Zhang X-O, Zhang J, Feng H, Dong R, Li X-J, *et al* (2015) ADAR1
763 is required for differentiation and neural induction by regulating microRNA processing in a
764 catalytically independent manner. *Cell Res* 25: 459–476

765 Conn SJ, Pillman KA, Toubia J, Conn VM, Salmanidis M, Phillips CA, Roslan S, Schreiber AW, Gregory PA
766 & Goodall GJ (2015) The RNA binding protein quaking regulates formation of circRNAs. *Cell* 160:
767 1125–1134

768 de la Mata M, Gaidatzis D, Vitanescu M, Stadler MB, Wentzel C, Scheiffele P, Filipowicz W & Großhans H
769 (2015) Potent degradation of neuronal miRNAs induced by highly complementary targets.
770 *EMBO Rep* 16: 500–511
771 Denzler R, Agarwal V, Stefano J, Bartel DP & Stoffel M (2014) Assessing the ceRNA hypothesis with
772 quantitative measurements of miRNA and target abundance. *Mol Cell* 54: 766–776
773 Denzler R, McGeary SE, Title AC, Agarwal V, Bartel DP & Stoffel M (2016) Impact of MicroRNA Levels,
774 Target-Site Complementarity, and Cooperativity on Competing Endogenous RNA-Regulated
775 Gene Expression. *Mol Cell* 64: 565–579
776 Dobin A, Davis CA, Schlesinger F, Drenkow J, Zaleski C, Jha S, Batut P, Chaisson M & Gingeras TR (2013)
777 STAR: ultrafast universal RNA-seq aligner. *Bioinformatics* 29: 15–21
778 Dodbele S, Mutlu N & Wilusz JE (2021) Best practices to ensure robust investigation of circular RNAs:
779 pitfalls and tips. *EMBO Rep* 22: e52072
780 Fellmann C, Hoffmann T, Sridhar V, Hopfgartner B, Muhar M, Roth M, Lai DY, Barbosa IAM, Kwon JS, Guan
781 Y, *et al* (2013) An optimized microRNA backbone for effective single-copy RNAi. *Cell Rep* 5:
782 1704–1713
783 Fuchs Wightman F, Giono LE, Fededa JP & de la Mata M (2018) Target RNAs Strike Back on MicroRNAs.
784 *Front Genet* 9: 435
785 Gasparini S, Licursi V, Presutti C & Mannironi C (2020) The Secret Garden of Neuronal circRNAs. *Cells* 9:
786 1815
787 Ghini F, Rubolino C, Climent M, Simeone I, Marzi MJ & Nicassio F (2018) Endogenous transcripts control
788 miRNA levels and activity in mammalian cells by target-directed miRNA degradation. *Nat*
789 *Commun* 9: 3119
790 Gibson DG, Young L, Chuang R-Y, Venter JC, Hutchison CA 3rd & Smith HO (2009) Enzymatic assembly
791 of DNA molecules up to several hundred kilobases. *Nat Methods* 6: 343–345
792 Giusti SA, Vogl AM, Brockmann MM, Vercelli CA, Rein ML, Trümbach D, Wurst W, Cazalla D, Stein V,
793 Deussing JM, *et al* (2014) MicroRNA-9 controls dendritic development by targeting REST. *Elife*
794 3: e02755
795 Glažar P, Papavasileiou P & Rajewsky N (2014) circBase: a database for circular RNAs. *RNA* 20: 1666–1670

796 Guarnerio J, Zhang Y, Cheloni G, Panella R, Mae Katon J, Simpson M, Matsumoto A, Papa A, Loretelli C,
797 Petri A, *et al* (2019) Intragenic antagonistic roles of protein and circRNA in tumorigenesis. *Cell*
798 *Res* 29: 628–640
799 Guo JU, Agarwal V, Guo H & Bartel DP (2014) Expanded identification and characterization of
800 mammalian circular RNAs. *Genome Biol* 15: 409
801 Han J, LaVigne CA, Jones BT, Zhang H, Gillett F & Mendell JT (2020) A ubiquitin ligase mediates target-
802 directed microRNA decay independently of tailing and trimming. *Science* 370: eabc9546
803 Hanan M, Simchovitz A, Yayon N, Vaknine S, Cohen-Fultheim R, Karmon M, Madrer N, Rohrlich TM,
804 Maman M, Bennett ER, *et al* (2020) A Parkinson's disease CircRNAs Resource reveals a link
805 between circSLC8A1 and oxidative stress. *EMBO Mol Med* 12: e11942
806 Hansen TB, Jensen TI, Clausen BH, Bramsen JB, Finsen B, Damgaard CK & Kjems J (2013) Natural RNA
807 circles function as efficient microRNA sponges. *Nature* 495: 384–388
808 Hansen TB, Wiklund ED, Bramsen JB, Villadsen SB, Statham AL, Clark SJ & Kjems J (2011) miRNA-
809 dependent gene silencing involving Ago2-mediated cleavage of a circular antisense RNA.
810 *EMBO J* 30: 4414–4422
811 Jeck WR, Sorrentino JA, Wang K, Slevin MK, Burd CE, Liu J, Marzluff WF & Sharpless NE (2013) Circular
812 RNAs are abundant, conserved, and associated with ALU repeats. *RNA* 19: 141–157
813 Jens M & Rajewsky N (2015) Competition between target sites of regulators shapes post-transcriptional
814 gene regulation. *Nat Rev Genet* 16: 113–126
815 Jonas S & Izaurralde E (2015) Towards a molecular understanding of microRNA-mediated gene
816 silencing. *Nat Rev Genet* 16: 421–433
817 Kingston ER, Blodgett LW & Bartel DP (2022) Endogenous transcripts direct microRNA degradation in
818 Drosophila, and this targeted degradation is required for proper embryonic development. *Mol*
819 *Cell*: S1097-2765(22)00849–8
820 Kleaveland B, Shi CY, Stefano J & Bartel DP (2018) A Network of Noncoding Regulatory RNAs Acts in the
821 Mammalian Brain. *Cell* 174: 350-362.e17
822 Kozomara A, Birgaoanu M & Griffiths-Jones S (2019) miRBase: from microRNA sequences to function.
823 *Nucleic Acids Res* 47: D155–D162

824 Kramer MC, Liang D, Tatomer DC, Gold B, March ZM, Cherry S & Wilusz JE (2015) Combinatorial control
825 of Drosophila circular RNA expression by intronic repeats, hnRNPs, and SR proteins. *Genes Dev*
826 29: 2168–2182
827 Kristensen LS, Andersen MS, Stagsted LVW, Ebbesen KK, Hansen TB & Kjems J (2019) The biogenesis,
828 biology and characterization of circular RNAs. *Nat Rev Genet* 20: 675–691
829 Krol J, Busskamp V, Markiewicz I, Stadler MB, Ribi S, Richter J, Duebel J, Bicker S, Fehling HJJ, Schubeler
830 D, *et al* (2010) Characterizing light-regulated retinal microRNAs reveals rapid turnover as a
831 common property of neuronal microRNAs. *Cell* 141: 618–631
832 Lee S, Song J, Kim S, Kim J, Hong Y, Kim Y, Kim D, Baek D & Ahn K (2013) Selective degradation of host
833 MicroRNAs by an intergenic HCMV noncoding RNA accelerates virus production. *Cell Host*
834 *Microbe* 13: 678–690
835 Li J-H, Liu S, Zhou H, Qu L-H & Yang J-H (2014) starBase v2.0: decoding miRNA-ceRNA, miRNA-ncRNA
836 and protein-RNA interaction networks from large-scale CLIP-Seq data. *Nucleic Acids Res* 42:
837 D92-97
838 Li L, Sheng P, Li T, Fields CJ, Hiers NM, Wang Y, Li J, Guardia CM, Licht JD & Xie M (2021) Widespread
839 microRNA degradation elements in target mRNAs can assist the encoded proteins. *Genes Dev*
840 35: 1595–1609
841 Li X, Liu C-X, Xue W, Zhang Y, Jiang S, Yin Q-F, Wei J, Yao R-W, Yang L & Chen L-L (2017) Coordinated
842 circRNA Biogenesis and Function with NF90/NF110 in Viral Infection. *Mol Cell* 67: 214-227.e7
843 Liang D & Wilusz JE (2014) Short intronic repeat sequences facilitate circular RNA production. *Genes and*
844 *Development* 28: 2233–2247
845 Liao Y, Smyth GK & Shi W (2014) featureCounts: an efficient general purpose program for assigning
846 sequence reads to genomic features. *Bioinformatics* 30: 923–930
847 Litke JL & Jaffrey SR (2019) Highly efficient expression of circular RNA aptamers in cells using
848 autocatalytic transcripts. *Nat Biotechnol* 37: 667–675
849 Liu CX, Li X, Nan F, Jiang S, Gao X, Guo SK, Xue W, Cui Y, Dong K, Ding H, *et al* (2019) Structure and
850 Degradation of Circular RNAs Regulate PKR Activation in Innate Immunity. *Cell* 177: 865-
851 880.e21

852 Love MI, Huber W & Anders S (2014) Moderated estimation of fold change and dispersion for RNA-seq
853 data with DESeq2. *Genome Biol* 15: 550
854 Marcinowski L, Tanguy M, Krmpotic A, Rädle B, Lisnić VJ, Tuddenham L, Chane-Woon-Ming B, Ruzsics Z,
855 Erhard F, Benkartek C, *et al* (2012) Degradation of cellular mir-27 by a novel, highly abundant
856 viral transcript is important for efficient virus replication in vivo. *PLoS Pathog* 8: e1002510
857 Memczak S, Jens M, Elefsinioti A, Torti F, Krueger J, Rybak A, Maier L, Mackowiak SD, Gregersen LH,
858 Munschauer M, *et al* (2013) Circular RNAs are a large class of animal RNAs with regulatory
859 potency. *Nature* 495: 333–338
860 Pamudurti NR, Bartok O, Jens M, Ashwal-Fluss R, Stottmeister C, Ruhe L, Hanan M, Wyler E, Perez-
861 Hernandez D, Ramberger E, *et al* (2017) Translation of CircRNAs. *Mol Cell* 66: 9-21.e7
862 Pawlica P, Moss WN & Steitz JA (2016) Host miRNA degradation by Herpesvirus saimiri small nuclear
863 RNA requires an unstructured interacting region. *RNA* 22: 1181–1189
864 Petkovic S, Graff S, Feller N, Berghaus J, Ruppert V-P, Dülfer J & Sczakiel G (2021) Circular versus linear
865 RNA topology: different modes of RNA-RNA interactions in vitro and in human cells. *RNA Biol*
866 18: 674–683
867 Pinzón N, Li B, Martinez L, Sergeeva A, Presumey J, Apparailly F & Seitz H (2017) microRNA target
868 prediction programs predict many false positives. *Genome Res* 27: 234–245
869 Piwecka M, Glažar P, Hernandez-Miranda LR, Memczak S, Wolf SA, Rybak-Wolf A, Filipchyk A, Klironomos
870 F, Cerda Jara CA, Fenske P, *et al* (2017) Loss of a mammalian circular RNA locus causes miRNA
871 deregulation and affects brain function. *Science* 357: eaam8526
872 Roditi I, Carrington M & Turner M (1987) Expression of a polypeptide containing a dipeptide repeat is
873 confined to the insect stage of Trypanosoma brucei. *Nature* 325: 272–274
874 Rybak-Wolf A, Stottmeister C, Glažar P, Jens M, Pino N, Giusti S, Hanan M, Behm M, Bartok O, Ashwal-
875 Fluss R, *et al* (2015) Circular RNAs in the Mammalian Brain Are Highly Abundant, Conserved,
876 and Dynamically Expressed. *Mol Cell* 58: 870–885
877 Salzman J, Chen RE, Olsen MN, Wang PL & Brown PO (2013) Cell-type specific features of circular RNA
878 expression. *PLoS genetics* 9: e1003777
879 Sanjana NE, Shalem O & Zhang F (2014) Improved vectors and genome-wide libraries for CRISPR
880 screening. *Nat Methods* 11: 783–784

881 Shalem O, Sanjana NE, Hartenian E, Shi X, Scott DA, Mikkelson T, Heckl D, Ebert BL, Root DE, Doench JG,
882 *et al* (2014) Genome-scale CRISPR-Cas9 knockout screening in human cells. *Science* 343: 84–87
883 Shi CY, Kingston ER, Kleaveland B, Lin DH, Stubna MW & Bartel DP (2020) The ZSWIM8 ubiquitin ligase
884 mediates target-directed microRNA degradation. *Science* 370: eabc9359
885 Simeone I, Rubolino C, Noviello TMR, Farinello D, Cerulo L, Marzi MJ & Nicassio F (2022) Prediction and
886 pan-cancer analysis of mammalian transcripts involved in target directed miRNA degradation.
887 *Nucleic Acids Res* 50: 2019–2035
888 Soutschek M, Gross F, Schratt G & Germain P-L (2022) scanMiR: a biochemically-based toolkit for
889 versatile and efficient microRNA target prediction. *Bioinformatics*: btac110
890 Tay Y, Rinn J & Pandolfi PP (2014) The multilayered complexity of ceRNA crosstalk and competition.
891 *Nature* 505: 344–352
892 The Galaxy platform for accessible, reproducible and collaborative biomedical analyses: 2022 update.
893 (2022) *Nucleic Acids Res* 50: W345-351
894 Vogl AM, Brockmann MM, Giusti SA, Maccarrone G, Vercelli CA, Bauder CA, Richter JS, Roselli F, Hafner
895 A-S, Dedic N, *et al* (2015) Neddylation inhibition impairs spine development, destabilizes
896 synapses and deteriorates cognition. *Nat Neurosci* 18: 239–251
897 Wickham H (2016) Data Analysis. In *ggplot2: Elegant Graphics for Data Analysis*, Wickham H (ed) pp 189–
898 201. Cham: Springer International Publishing
899 Wickham H, Averick M, Bryan J, Chang W, McGowan LD, François R, Grolemund G, Hayes A, Henry L,
900 Hester J, *et al* (2019) Welcome to the Tidyverse. *Journal of Open Source Software* 4: 1686
901 Wickham H & Bryan J (2022) readxl: Read Excel Files. *https://readxl.tidyverse.org,*
902 *https://github.com/tidyverse/readxl*
903 Xiao M-S, Ai Y & Wilusz JE (2020) Biogenesis and Functions of Circular RNAs Come into Focus. *Trends Cell*
904 *Biol* 30: 226–240
905 Yang J-H, Li J-H, Shao P, Zhou H, Chen Y-Q & Qu L-H (2011) starBase: a database for exploring microRNA-
906 mRNA interaction maps from Argonaute CLIP-Seq and Degradome-Seq data. *Nucleic Acids Res*
907 39: D202-209

908 You X, Vlatkovic I, Babic A, Will T, Epstein I, Tushev G, Akbalik G, Wang M, Glock C, Quedenau C, *et al*
909 (2015) Neural circular RNAs are derived from synaptic genes and regulated by development
910 and plasticity. *Nat Neurosci* 18: 603–610
911 Zhang XO, Wang H Bin, Zhang Y, Lu X, Chen LL & Yang L (2014) Complementary sequence-mediated
912 exon circularization. *Cell* 159: 134–147
913 Zhang Y, Xue W, Li X, Zhang J, Chen S, Zhang J-L, Yang L & Chen L-L (2016) The Biogenesis of Nascent
914 Circular RNAs. *Cell Rep* 15: 611–624
915

916 # Figure legends

917 **Figure 1.**

918 **System to artificially express circRNAs reducing their overlapping, cognate linear RNA**
919 **expression.**

920 A. Top: Illustration of the linear RNA expressing construct used as a positive control for TDMD (TDMD
921 inducer). Bottom: Illustration of the circRNA-expressing construct; depicted with coloured arrows
922 are the sets of primers used to measure the different transcript variants (circular [1], Total Output-
923 TO [2] and linear [3]).

924 B. Total output (TO), linear and circular RNA levels upon expression of the circRNA-expressing
925 constructs from the tetracycline-inducible promoter (TREp) bearing perfectly matched or seed-
926 mutant miR-124 sites for selective linear RNA degradation (see Figure EV1A). n = 5 culture wells
927 (from 3 independent primary cultures) of cortical neurons for each condition; and n = 7 culture
928 wells (from 4 independent primary cultures) of hippocampal neurons for each condition.

929 C. Total reporter output (left) and circRNA levels (right) upon expression of the circRNA-expressing
930 construct or the linear RNA construct (TDMD inducer). The constructs were expressed from the
931 tetracycline-inducible promoter (TREp) and the synapsin (Syn) promoter respectively in order to
932 achieve similar total output levels for both constructs n = 9 culture wells (from 3 independent
933 primary cultures) of cortical neurons for each condition; n = 9 culture wells (from 4 independent
934 primary cultures) of hippocampal neurons for each condition. Missing points are failed culture
935 wells/RT-qPCR reactions.

936 In (B–C), data are presented as mean ± SEM. Statistical significance was determined by unpaired
937 Student's *t* tests (ns: $p > 0.05$, *: $p <= 0.05$, **: $p <= 0.01$, ***: $p <= 0.001$, ****: $p <= 0.0001$).

938

939 **Figure 2.**

940 **Artificial circRNA-expressing constructs are unable to trigger TDMD.**

941 A MiR-132 abundance upon transduction of the linear control (left) or the circRNA-expressing
942 construct (right) carrying bulged (TDMD-compatible) or seed-mutant miR-132 sites. n = 9 culture
943 wells (from 3 independent primary cultures) of cortical neurons for each condition; n = 9 culture

944 wells (from 4 independent primary cultures) of hippocampal neurons for each condition. Missing
945 points are failed culture wells/RT-qPCR reactions.
946 B AGO2-Flag immunoprecipitation (RIP) followed by RT-qPCR in HEK293T cells. MiR-27a was used to
947 normalize expression. Relative circRNA abundance was measured using circRNA-backspliced-
948 junction specific divergent primers and normalized to miR-27a levels as an unrelated RISC-loaded
949 miRNA not expected to be affected by the circRNA. Levels of non-specific *U6* background binding
950 to Ago2 are shown. As an IP quality control, FLAG/HA-AGO2 input levels were shown to be similar
951 across transfected conditions and efficiently pulled-down using anti-FLAG beads (Figure EV2B).
952 Accordingly, miR-27, but not *U6* RNA, was efficiently co-immunoprecipitated, showing an even
953 recovery of Ago-bound RNA across transfected conditions (Figure EV2C). n = 4 culture wells (from
954 2 experiments) of HEK293T cells for each condition.
955 C Subcellular fractionation showing total vs. cytoplasmic (left) and total vs. nuclear (right) fractions,
956 followed by RT-qPCR of the circRNA and linear RNA isoforms, normalized by *GAPDH* (for cytoplasm)
957 or *U6* (for nucleus). Fractionation efficiency was assessed via Western Blot and RT-qPCR (Figure
958 EV2D-E). n = 4 culture wells (from 2 experiments) of HEK293T cells for each condition.
959 In (A–C), data are presented as mean ± SEM . Statistical significance was determined by unpaired
960 Student's *t tests* (ns: p > 0.05, *: p <= 0.05, **: p <= 0.01, ***: p <= 0.001, ****: p <= 0.0001).
961
962 **Figure 3.**
963 **The topology of *Cdr1as* determines the outcome of its effect on miR-7's stability.**
964 A *Cdr1as* total output levels (linear plus circular) measured by RT-qPCR upon transduction of either
965 a scrambled shRNA or sh*Cdr1as* alone, or sh*Cdr1as* rescued with a linear version of *Cdr1as*
966 (lin*Cdr1as*) lacking the *shCdr1as* site, in cortical primary neurons. n = 6 culture wells (from 3
967 independent primary cultures) for control and cirCDR1as KD; n = 4 culture wells (from 2
968 independent primary cultures) for lin*Cdr1as* rescue.
969 B MiR-7 abundance measured by Taqman RT-qPCR in the same samples as in A. n = 6 culture wells
970 (from 3 independent primary cultures) for control and cirCDR1as KD; n = 4 culture wells (from 2
971 independent primary cultures) for lin*Cdr1as* rescue.

972 C *Cdr1as* total output levels measured by RT-qPCR upon over-expression of linear *Cdr1as* (lin*Cdr1as*)
973 in primary hippocampal neurons. Control corresponds to a non-related (GFP-expressing) linear
974 transcript. n = 6 culture wells (from 2 independent primary cultures) for each condition.
975 D MiR-7 abundance measured by Taqman RT-qPCR in the same samples as in C. n = 6 culture wells
976 (from 2 independent primary cultures) for each condition.
977 Data are presented as mean ± SEM. Statistical significance was determined by unpaired Student's *t tests*
978 (ns: p > 0.05, *: p <= 0.05, **: p <= 0.01, ***: p <= 0.001, ****: p <= 0.0001).
979
980 **Figure 4.**
981 **CircRNAs potentially stabilize dozens of microRNAs across neuron-like differentiation.**
982 A Scatter plot of miRNA expression fold changes (log2) across differentiation of hESC H9 cells into
983 forebrain (FB) neuron progenitor cells plotted against the number of effective sites, coloured by
984 quartiles of increasing number of "effective" sites within circRNAs.
985 B Scatter plot of miRNA fold changes (log2) across differentiation plotted against miRNA "sponging
986 suffered" coefficient score (log10) coloured by quartiles in a scatter plot. The predicted most highly
987 "sponged" miRNAs show the highest fold changes across differentiation.
988 C Boxplot depicting the fold changes (log2) across differentiation of miRNA separated by quartiles
989 of increasing "sponging suffered" coefficients.
990 D Scatter plots of miRNA fold changes (log2) plotted against pri-miRNA fold changes (log2) faceted
991 by "sponging suffered" coefficient quartiles. Indicated are the slopes (b) and p-values for the
992 interaction terms of each quartile's curve against the reference ("-sponged") quartile within a
993 multiple regression model with interaction.
994 E Boxplot showing circRNA expression fold changes (log2) across differentiation separated by
995 quartiles of increasing "sponging capacity " index.
996 The analysis includes 236 miRNAs. For panels C and E, GLM with emmeans statistics are shown between
997 the least sponged and the remaining groups (ns: p > 0.05, *: p <= 0.05, **: p <= 0.01, ***: p <= 0.001,
998 ****: p <= 0.0001).
999
1000 **Figure 5.**

1001 **Predicted TDMD-like site architectures within circRNAs are more frequent for the most highly**
1002 **"sponged" miRNAs**

1003 A Pie charts showing the proportion of linear RNA- and circRNA-miRNA interactions involving at least
1004 one predicted TDMD-like site against miRNAs within quartiles of increasing "sponging suffered"
1005 coefficients. Shown are the p-values for the Fisher's Exact test between each quartile and the least
1006 sponged quartile ("- sponged").

1007 B Violin plots depicting the number of predicted TDMD-like sites within circRNAs against miRNAs
1008 belonging to quartiles of increasing "sponging suffered" coefficients. GLM with emmeans statistics
1009 are shown between the least sponged and the other quartiles (ns: $p > 0.05$, *: $p <= 0.05$, **: $p <=$
1010 0.01, ***: $p <= 0.001$, ****: $p <= 0.0001$).

1011

1012 Expanded View Figure Legends

1013 **Figure EV1.**

1014 **CircRNA-expressing constructs and quality controls.**

1015 A Table summarizing the generated constructs.

1016 B Northern blot analysis of RNase R treated or untreated samples from HEK293T cells expressing the
1017 indicated constructs. CircRNAs are resistant to RNase R digestion, confirming the circular topology
1018 of the artificial circRNA. All constructs were expressed from the tetracycline-inducible promoter
1019 (TREp). The asterisk (*) marks a putative mechanically linearized product of the corresponding
1020 circRNA.

1021 C Quantification by different methods of the linear and circular isoforms from RNase R untreated
1022 samples of HEK293T cells (naturally lacking miR124) expressing the indicated constructs. Top
1023 panels: digital densitometry quantification of Northern blot bands by ImageJ. Bottom panels: RT-
1024 qPCR quantification using primers specific for the circular isoform or for both the linear and circular
1025 isoforms combined (Total output) as depicted in Figure 1A. In red, the mean is indicated. n = 2
1026 culture wells (from 1 experiment) of HEK293T cells for each condition.

1027 D RT-qPCR measurement of the circRNA-to-linear RNA ratio of RNase R treated vs. untreated samples
1028 in cortical neurons or HEK293T cells using divergent primers depicted in Figure 1. Values reflect
1029 relative rather than absolute ratios of the measured isoforms. n = 3 culture wells (from 1 primary

1030 culture/experiment) of each cell type and for each condition.E Top: Agarose gel showing
1031 triplicates of the qPCR amplicons obtained with divergent primers against the backsplicing
1032 junction of the artificial circRNA, after retro-transcription with two different reverse transcriptases
1033 (MMLV-RT & Superscript II) in order to rule out artifacts due to template switching during cDNA
1034 synthesis. Bottom: Sanger sequencing of the amplicons shown above confirming backsplicing
1035 junction in HEK293 cells.
1036
1037 **Figure EV2.**
1038 **TDMD specificity, HA-FLAG/AGO2 RIP and cellular fractionation quality controls.**
1039 A RT-qPCR quantification of the indicated RNA species confirms specific degradation of miR-132
1040 guide strand (miR-132-3p) and discards potential transcriptional effects. Levels of miR-132
1041 passenger strand (miR-132-5p), primary transcript (pri-miR-132) and four unrelated miRNAs (miR-
1042 124-3p, miR-128-3p, miR-138-5p and miR-409-3p) were normalized to *U6*. n = 9 culture wells (from
1043 3 independent primary cultures) of cortical neurons for each condition; n = 9 culture wells (from 4
1044 independent primary cultures) of hippocampal neurons for each condition. Missing points are
1045 failed culture wells/RT-qPCR reactions.
1046 B Representative anti-HA Western Blot from inputs or anti-FLAG IPs in non-transfected HEK-293T
1047 cells or cells co-transfected with HA-FLAG/AGO2 and the circRNA-expressing construct bearing
1048 bulged (WT) or seed-mutant (mut) miR-132 sites.
1049 C *U6* and miR-27 levels were measured to verify the efficiency of HA-FLAG/AGO2
1050 immunoprecipitation. n = 4 culture wells (from 2 experiments) of HEK293T cells for each condition.
1051 D Representative Western Blot of HEK293T cells transfected with either the circRNA-expressing
1052 construct or the linear control RNA, following subcellular fractionation. β-Tubulin and Histone-3
1053 were used as cytoplasm and nucleus markers, respectively.
1054 E Boxplot depicting median values of *GAPDH*/*U6* ratio measured by RT-qPCR confirms proper
1055 subcellular fractionation of samples either transfected with the circRNA-expressing construct or
1056 the linear control. n = 4 culture wells (from 1 experiment) of HEK293T cells for each condition.

1057 In (A, C), data are presented as mean ± SEM. Statistical significance was determined by unpaired
1058 Student's *t tests* (ns: p > 0.05, *: p <= 0.05, **: p <= 0.01, ***: p <= 0.001, ****: p <= 0.0001). In panel
1059 A, Bonferroni's correction for multiple testing was applied.
1060
1061 **Figure EV3.**
1062 **MicroRNA site illustrations, quality controls and primer design for *Cdr1as*.**
1063 A Scheme depicting the sequences of the miR-671 binding site within *Cdr1as*, miR-671 and the
1064 engineered sh*Cdr1as*. The latter is based on miR-671 with two nucleotide changes that make it
1065 fully complementary to the circRNA to maximize its slicing capacity.
1066 B Three examples of potential TDMD-competent binding sites for miR-7 present in *Cdr1as*, aligned
1067 and illustrated using scanMiR.
1068 C Expression levels of *Cdr1as* total output, circular *Cdr1as* and unrelated gene (*Actb*) upon over-
1069 expression of linear *Cdr1as* (lin*Cdr1as*). Levels were normalized to *Gapdh*. n = 6 culture wells (from
1070 2 independent primary cultures) for each condition.
1071 D Expression levels of miR-7 guide strand (miR-7-5p), passenger strands (miR-7a-1-3p and miR-7a-2-
1072 3p), primary RNA (pri-miR-7a-1) and two unrelated miRNAs (miR-9-5p and miR-132-3p). All miRNAs
1073 levels were normalized to *U6*, while the pri-miR level was normalized to *Gapdh*. n = 6 culture wells
1074 (from 2 independent primary cultures) for each condition.
1075 E Illustration of the strategy designed to mutate *Cdr1as* splicing sites by CRISPR/Cas9.
1076 F *Cdr1as* total output levels upon CRISPR/Cas9 editing of the *Cdr1as* splicing sites, measured by RT-
1077 qPCR in primary hippocampal neurons. Control corresponds to a transduced linear transcript (GFP-
1078 expressing). n = 3 culture wells (from 1 independent primary culture) for each condition.
1079 G MiR-7 abundance measured by Taqman RT-qPCR in the same samples as in F. n = 3 culture wells
1080 (from 1 independent primary culture) for each condition.
1081 H Illustration of the primer designs for measuring the different *Cdr1as* isoforms (detailed in Materials
1082 and Methods).
1083 Data are presented as mean ± SEM. Statistical significance was determined by unpaired Student's *t tests*
1084 (ns: p > 0.05, *: p <= 0.05, **: p <= 0.01, ***: p <= 0.001, ****: p <= 0.0001). In panels C and D, Bonferroni's
1085 correction for multiple testing was applied. For the F and G panels, equal variance was assumed.

1086

1087 **Figure EV4.**

1088 **Illustrations of the predicted circRNA-miRNA networks and genomic features of the potentially**

1089 **involved circRNAs.**

1090 A Network diagram of biochemically supported interactions between circRNAs and miRNAs.

1091 Depicted are the interactions involving the seven most "sponging" circRNAs.

1092 B Network diagram showing biochemically supported circRNA-miRNA interactions for miR-7 and

1093 two other miRNAs with similar "sponging" coefficient (miR-670-3p and miR-409-3p). For all three

1094 examples, the stoichiometries (i.e. ratios of circRNA-binding-site:miRNA) are similar, with CDR1as

1095 making the largest contribution for miRNA-7. MiR-7 and miR-409 are also a demonstrated case and

1096 strong candidate to undergo of TDMD, respectively (see main text).

1097 C Boxplot showing the size of circRNAs (log2 of the base pairs) that interact with miRNAs from each

1098 of the different "sponging" quartiles. Shown are Wilcoxon rank sum test p-values (corrected with

1099 the Hochberg method for multiple comparisons) between the least sponged and the remaining

1100 groups (ns: $p > 0.05$).

1101 D Barplot representing the percentages of overlapping genomic regions (CDS, 5'UTR, 3'UTR, etc)

1102 giving rise to the circRNAs with predicted binding sites against miRNAs within different quartiles

1103 of sponging suffered. No enrichment of genomics features for circRNAs interacting with miRNAs

1104 within the different quartiles was observed (Pearson's Chi-squared test p-value = 0.998).

1105

1106 **Figure EV5.**

1107 **Examples of predicted TDMD-like sites on circRNAs.**

1108 A-B Pie charts showing the proportion of and circRNA-miRNA (A) and linear RNA-miRNA (B)

1109 interactions involving at least one predicted TDMD-like site against miRNAs within quartiles of

1110 increasing "sponging suffered" coefficients. Shown are the p-values for the Fisher's Exact test

1111 between each quartile and the least sponged quartile ("- sponged").

1112

1113 C Examples of TDMD-like sites within circRNAs predicted and aligned using scanMiR. The five

1114 miRNAs belong to the "+++ sponged" quartile.

1115

Figure 1

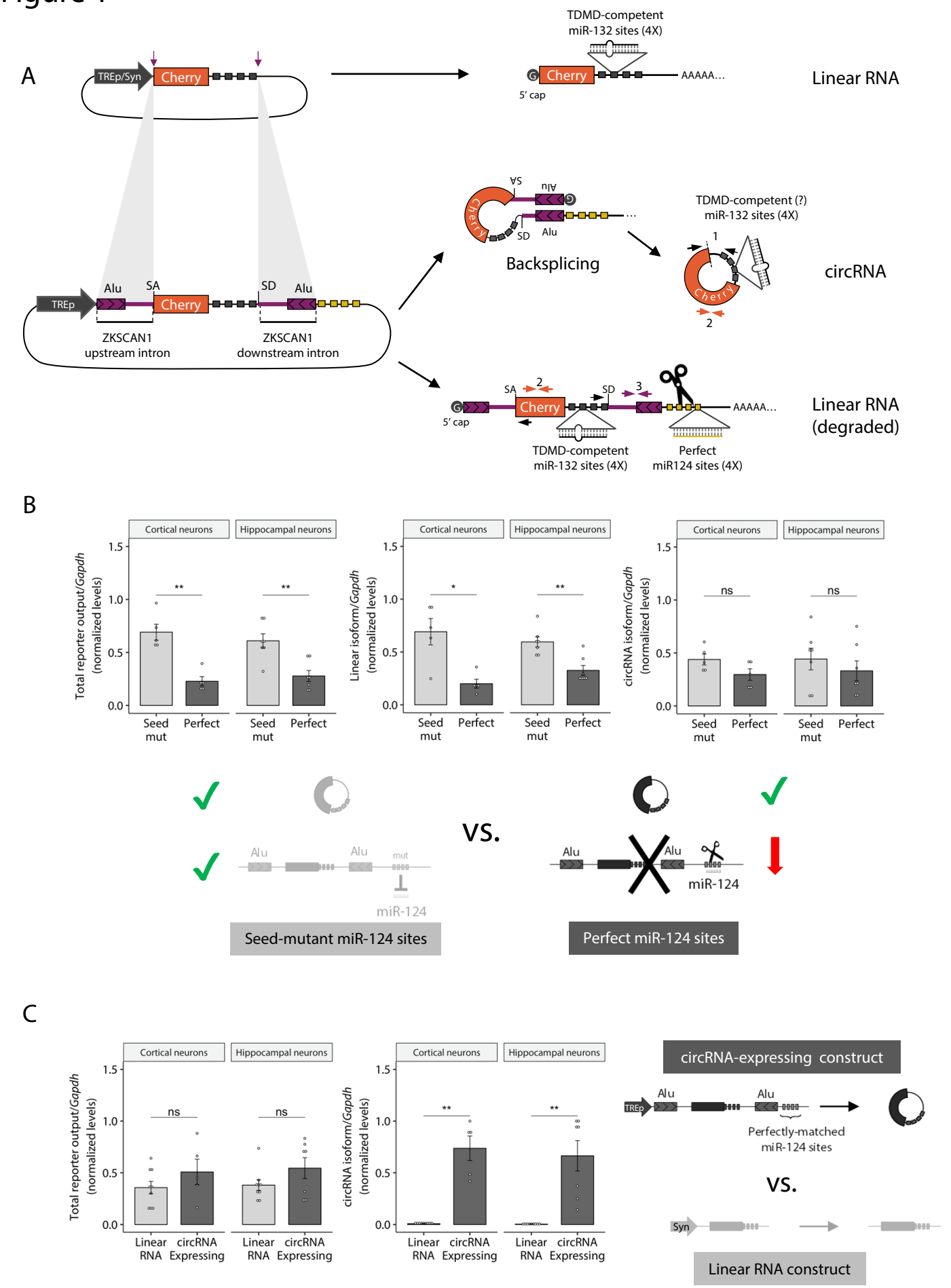
A
TREp/Syn
Cherry
TDMD-competent
miR-132 sites (4X)
Cherry
AAAAA...
5' cap
Linear RNA
TREp
Alu
SA
Cherry
SD
Alu
ZKSCAN1
upstream intron
ZKSCAN1
downstream intron
SA
Alu
Cherry
SD
Alu
Backsplicing
TDMD-competent (?)
miR-132 sites (4X)
1
2
circRNA
SA
2
SD
3
Cherry
AAAAA...
5' cap
TDMD-competent
miR-132 sites (4X)
Perfect
miR124 sites (4X)
Linear RNA
(degraded)
B
Cortical neurons
Hippocampal neurons
Total reporter output/Gapdh
(normalized levels)
Linear isoform/Gapdh
(normalized levels)
circRNA isoform/Gapdh
(normalized levels)
Seed mut
Perfect
ns
Alu
mut
miR-124
vs.
Seed-mutant miR-124 sites
Perfect miR-124 sites
C
Cortical neurons
Hippocampal neurons
Total reporter output/Gapdh
(normalized levels)
circRNA isoform/Gapdh
(normalized levels)
Linear RNA
circRNA Expressing
ns
circRNA-expressing construct
TREp
Alu
Perfectly-matched
miR-124 sites
vs.
Syn
Linear RNA construct

Figure 2

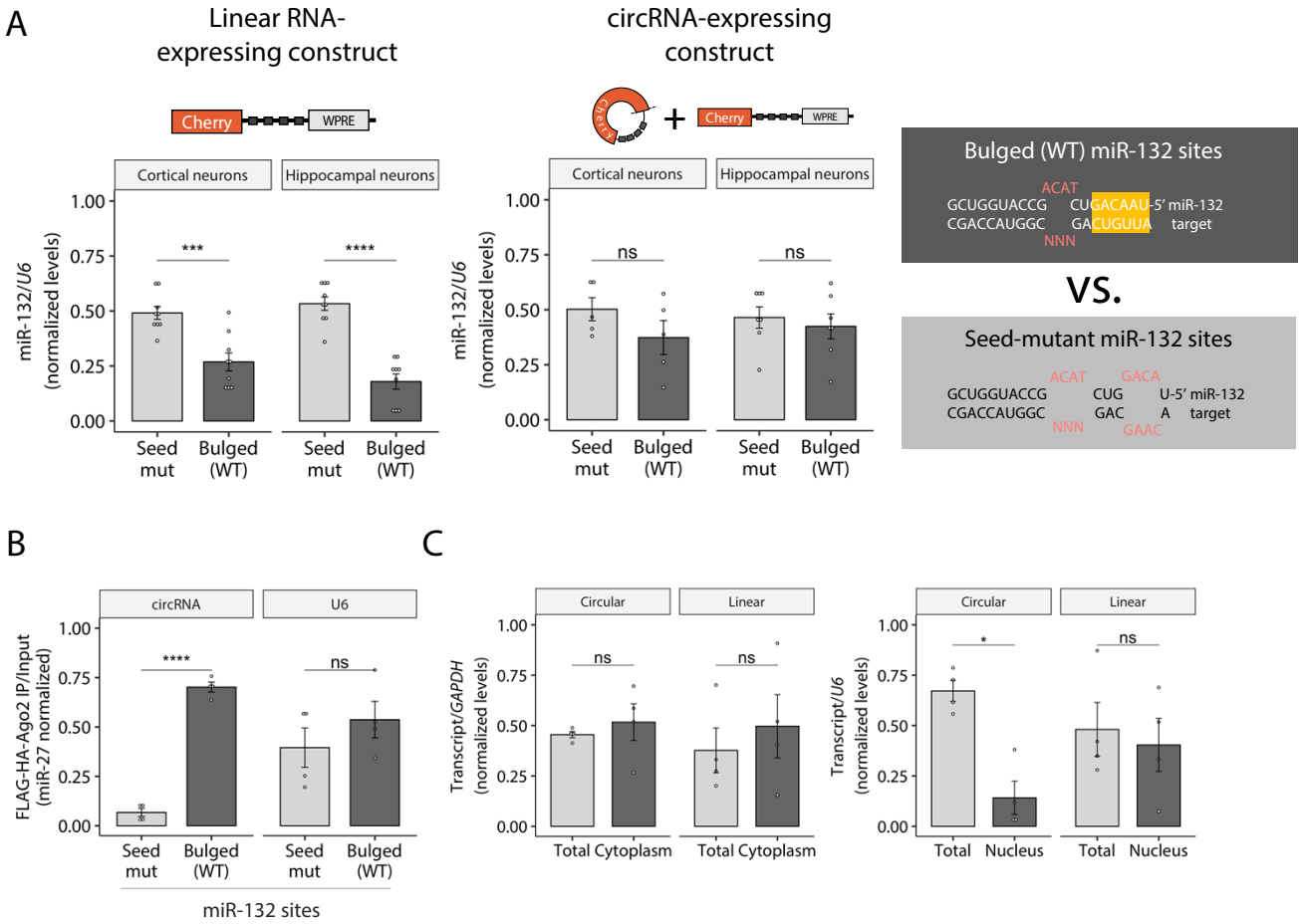
A
Linear RNA-expressing construct
circRNA-expressing construct
Cherry
WPRE
Cortical neurons
Hippocampal neurons
miR-132/U6 (normalized levels)
1.00
0.75
0.50
0.25
0.00
***
****
ns
Seed mut
Bulged (WT)
Bulged (WT) miR-132 sites
ACAT
GCUGGUACCG
CGACCAUGGC
CUGACAAU
GACUGUUA
5′ miR-132
target
NNN
VS.
Seed-mutant miR-132 sites
ACAT
GACA
GCUGGUACCG
CGACCAUGGC
CUG
GAC
U-5′ miR-132
A
target
NNN
GAAC
B
circRNA
U6
FLAG-HA-Ago2 IP/Input (miR-27 normalized)
miR-132 sites
C
Circular
Linear
Transcript/GAPDH (normalized levels)
Total
Cytoplasm
Transcript/U6 (normalized levels)
Nucleus

Figure 3

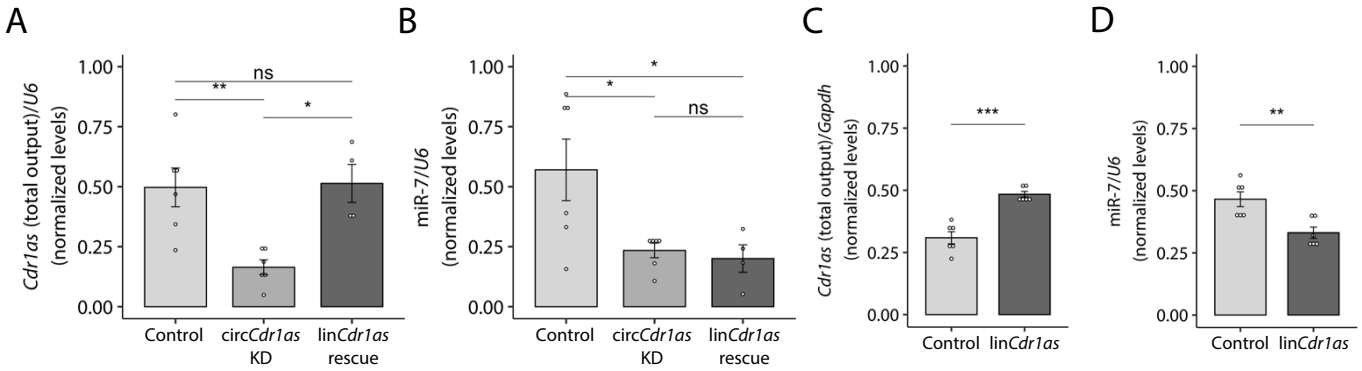
A
B
C
D
Cdr1as (total output)/U6 (normalized levels)
miR-7/U6 (normalized levels)
Cdr1as (total output)/Gapdh (normalized levels)
miR-7/U6 (normalized levels)
1.00
0.75
0.50
0.25
0.00
ns
**
*
***
Control
circCdr1as KD
linCdr1as rescue
linCdr1as

Figure 4

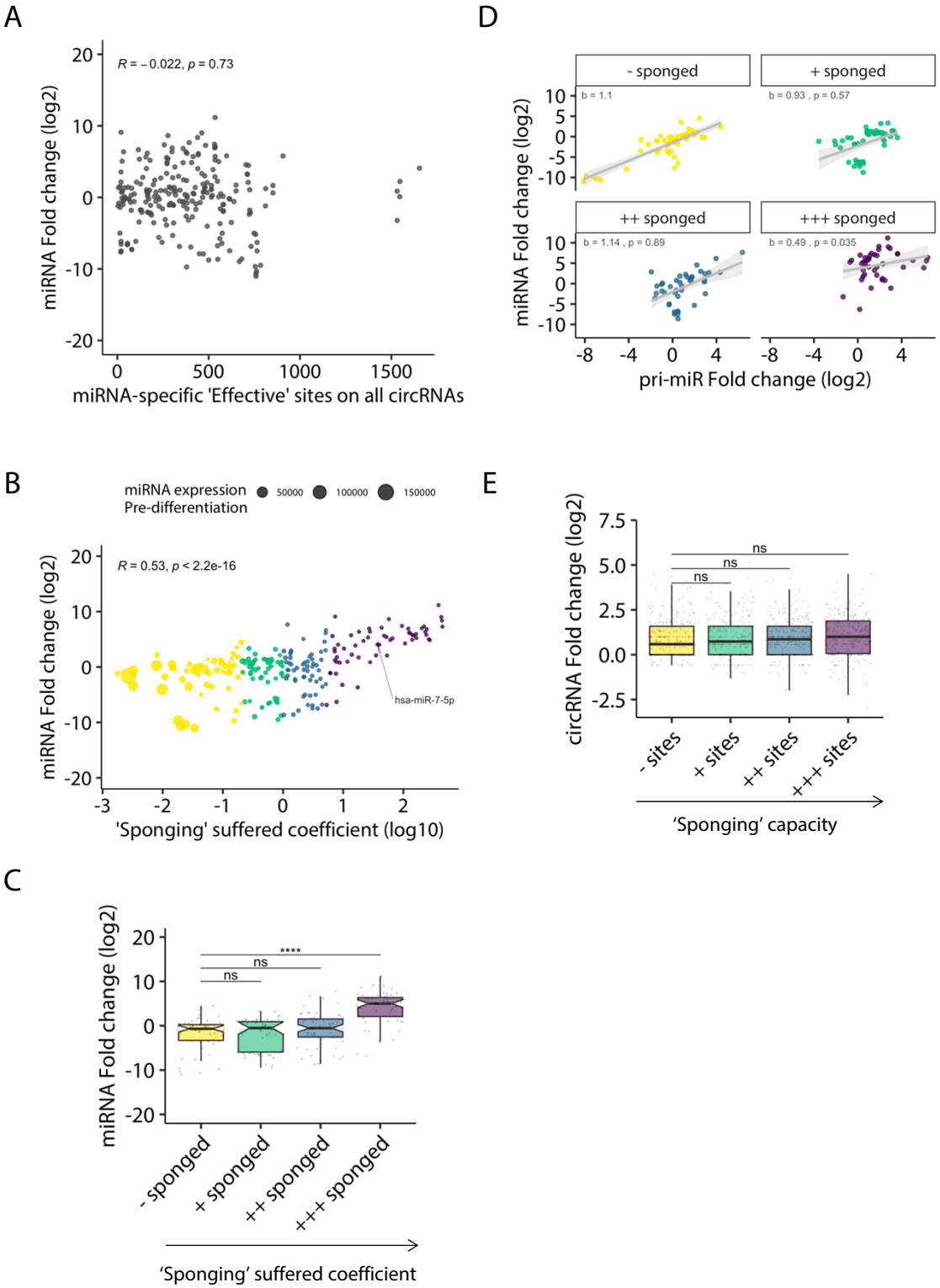
A
R = −0.022, p = 0.73
miRNA Fold change (log2)
miRNA-specific 'Effective' sites on all circRNAs
D
- sponged
+ sponged
++ sponged
+++ sponged
b = 1.1
b = 0.93 , p = 0.57
b = 1.14 , p = 0.89
b = 0.49 , p = 0.035
miRNA Fold change (log2)
pri-miR Fold change (log2)
B
miRNA expression
Pre-differentiation
50000
100000
150000
R = 0.53, p < 2.2e-16
hsa-miR-7-5p
miRNA Fold change (log2)
'Sponging' suffered coefficient (log10)
E
circRNA Fold change (log2)
ns
- sites
+ sites
++ sites
+++ sites
'Sponging' capacity
C
miRNA Fold change (log2)
****
ns
- sponged
+ sponged
++ sponged
+++ sponged
'Sponging' suffered coefficient

Figure 5

A

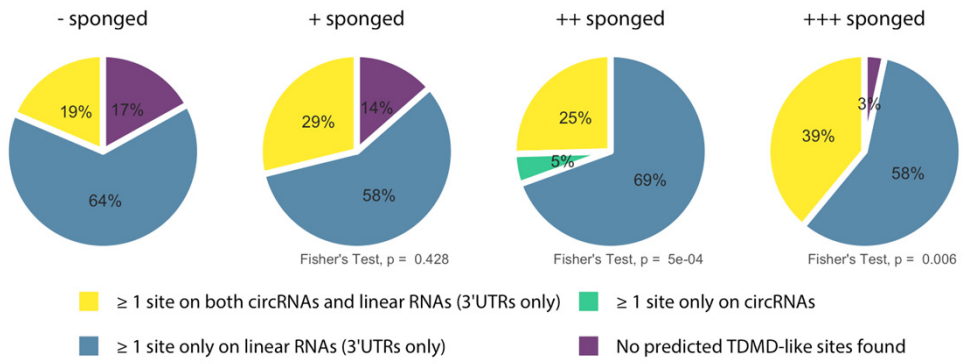
- sponged
+ sponged
++ sponged
+++ sponged
19%
17%
64%
29%
14%
58%
25%
5%
69%
3%
39%
58%
Fisher's Test, p = 0.428
Fisher's Test, p = 5e-04
Fisher's Test, p = 0.006
≥ 1 site on both circRNAs and linear RNAs (3'UTRs only)
≥ 1 site only on circRNAs
≥ 1 site only on linear RNAs (3'UTRs only)
No predicted TDMD-like sites found

B

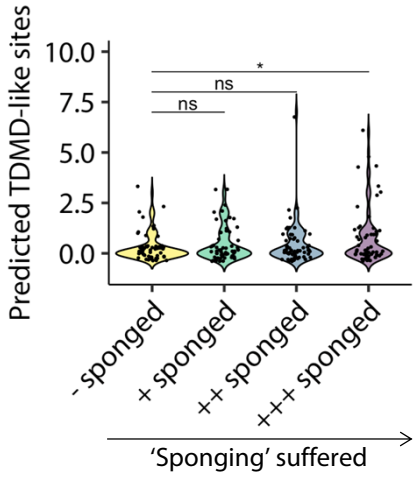
Predicted TDMD-like sites
10.0
7.5
5.0
2.5
0.0
*
ns
ns
- sponged
+ sponged
++ sponged
+++ sponged
'Sponging' suffered